bioRxiv preprint doi: https://doi.org/10.1101/323956; this version posted May 16, 2018. The copyright holder for this preprint (which was not certified by peer review) is the author/funder. All rights reserved. No reuse allowed without permission.

An insulin, AMPK, and steroid hormone-mediated metabolic switch regulates the transition between growth and diapause in *C. elegans*

Sider Penkov[1], Cihan Erkut[1*], Jana Oertel[2], Roberta Galli[3], Daniela Vorkel[1], Jean-Marc Verbavatz[1,4], Edmund Koch[3], Karim Fahmy[2] and Teymuras V. Kurzchalia[1]

1. Max Planck Institute of Molecular Cell Biology and Genetics, Dresden, Germany
2. Institute of Resource Ecology at the Helmholtz-Zentrum Dresden-Rossendorf, Dresden, Germany
3. TU Dresden, Faculty of Medicine Carl Gustav Carus, Department of Anesthesiology and Intensive Care Medicine, Clinical Sensoring and Monitoring, Dresden, Germany
4. Institut Jacques Monod, Université Paris Diderot, Paris, France

*Current address: European Molecular Biology Laboratory, Heidelberg, Germany

Correspondance to:

Teymuras Kurzchalia, PhD
MPI-CBG
Pfotenhauerstr. 108
01307 Dresden, Germany
Tel.: +49 351 210 2567
Fax: +49 351 210 1489
E-mail: kurzchalia@mpi-cbg.de

or

Sider Penkov, PhD
Paul Langerhans Institute Dresden
Fetscherstr. 74
01307 Dresden, Germany
Tel.: +49 351 796 36618
Fax: +49 351 796 36699
E-mail: sider.penkov1@tu-dresden.de

Lead contact: Teymuras Kurzchalia

bioRxiv preprint doi: https://doi.org/10.1101/323956; this version posted May 16, 2018. The copyright holder for this preprint (which was not certified by peer review) is the author/funder. All rights reserved. No reuse allowed without permission.

Abstract

The ability of organisms to adapt to environmental changes and regulate the balance between growth and quiescence depend on global transitions in metabolic state. Under harsh environmental conditions, *C. elegans* enters diapause and forms a specialized dauer larva. This larva has a specific morphology and its metabolism switches from the tricarboxylic acid (TCA) cycle to gluconeogenesis. Here, we show that these changes involve concerted activity of several regulatory pathways. Whereas the insulin pathway maintains low energy expenditure through the FoxO transcription factor DAF-16, dauer morphogenesis is controlled by the steroid hormone receptor DAF-12. We show that downstream or in parallel to DAF-16 operates the AMPK α-subunit AAK-2. AAK-2 and DAF-12 separately promote a switch from TCA cycle to gluconeogenesis, serving as metabolic "turnouts to a slow lane". When both are suppressed, the TCA cycle is active and the developmental arrest is abolished. Thus, a global metabolic switch governs the transition between growth and quiescence.

bioRxiv preprint doi: https://doi.org/10.1101/323956; this version posted May 16, 2018. The copyright holder for this preprint (which was not certified by peer review) is the author/funder. All rights reserved. No reuse allowed without permission.

Introduction

Throughout their life cycle, organisms alternate between states of high and low metabolic activity. Metabolic activity after feeding, for instance, differs significantly from that observed during high physical activity or sleep. Under extreme conditions such as freezing or desiccation, some organisms can enter a so-called cryptobiotic state in which metabolism is reduced to undetectable levels, allowing them to survive for very long periods of time (Erkut and Kurzchalia, 2015). In some cases, however, not only the intensity but the whole mode of metabolism changes, for instance during the transition from growth to quiescence. Usually, growing organisms have highly active mitochondria and intensive oxidative phosphorylation (OXPHOS), whereas during metabolic quiescence they shift to glycolysis and associated gluconeogenesis (Hand et al., 2016). Interestingly, most early embryos use glycolytic metabolism and only shift to OXPHOS during later phases of development (Smith and Sturmey, 2013). This metabolic shift is also observed during the differentiation of neurons and stem cells (Homem et al., 2014; Ito and Suda, 2014), whereas the opposite change, from OXPHOS to glycolysis, is seen in cancer cells exhibiting "Warburg" metabolism (Cairns et al., 2011; Warburg, 1956). It is known that cancer cells maintain an aerobic glycolytic mode with significantly diminished OXPHOS. Despite their importance, however, we still have a limited understanding of mechanisms controlling these global metabolic transitions.

Entry of the nematode *Caenorhabditis elegans* into diapause is an excellent model in which to study global metabolic transitions. In response to harsh environmental conditions, *C. elegans* interrupts its reproductive life cycle, stops growing and forms a specialized, developmentally arrested third larval stage called a dauer (enduring) larva (Riddle, 1988). The body of dauer larvae is morphologically

bioRxiv preprint doi: https://doi.org/10.1101/323956; this version posted May 16, 2018. The copyright holder for this preprint (which was not certified by peer review) is the author/funder. All rights reserved. No reuse allowed without permission.

adapted to harsh conditions. Its diameter is reduced, its body coated with a tight cuticle, and its pharynx sealed (Cassada and Russell, 1975; Riddle et al., 1981; Vowels and Thomas, 1992). Most importantly, the metabolism of dauer larvae differs substantially from that of the reproductive L3 stage. Since they do not feed, they rely on stored energy reserves (Riddle, 1988). To restrict the fast depletion of these reserves, dauer larvae enter a hypometabolic mode via a dramatic rearrangement of anabolic and catabolic pathways. In this "stand-by" mode, energy consumption, heat production, aerobic respiration and TCA cycle activity are significantly reduced. The production of cofactors required for anabolic reactions such as NADPH is also kept at minimum (Penkov et al., 2015). In addition, the glyoxylate shunt and gluconeogenesis are used to generate carbohydrates from reserve lipids (Burnell et al., 2005; Erkut et al., 2016; Erkut and Kurzchalia, 2015; Houthoofd et al., 2002; Vanfleteren and De Vreese, 1996; Wadsworth and Riddle, 1989). In this state, dauers can survive for months without nutrition.

The process of dauer formation is controlled by Daf genes (from dauer formation). Whereas Daf-c mutants constitutively undergo dauer arrest, Daf-d mutants are defective in forming dauer larvae. Genetic analysis of Daf mutants has revealed that dauer formation is governed by several signaling pathways: guanylyl cyclase, TGF-β-like, insulin-like and steroid hormone pathways (**Figure 1A**) (Antebi, 2013b; Riddle, 1988). In response to changes in population density (sensed through dauer-inducing pheromones) and altered energetic metabolism (signaled by insulin-like peptides), the guanylyl cyclase, TGF-β and insulin-like signaling pathways converge on two transcription factors: the FoxO member DAF-16 and the nuclear hormone receptor DAF-12, both encoded by Daf-d genes. DAF-16 is genetically negatively regulated by the insulin receptor homolog DAF-2 in response to

bioRxiv preprint doi: https://doi.org/10.1101/323956; this version posted May 16, 2018. The copyright holder for this preprint (which was not certified by peer review) is the author/funder. All rights reserved. No reuse allowed without permission.

stimulation of the latter by insulin-like peptides (Henderson and Johnson, 2001; Lee et al., 2001; Lin et al., 2001). DAF-12, on the other hand, is regulated by steroid hormones, called dafachronic acids (DAs), synthesized by the cytochrome P450 enzyme DAF-9 when the population density and the concentration of dauer-inducing pheromones are low (Butcher, 2017; Fielenbach and Antebi, 2008; Motola et al., 2006; Riddle and Albert, 1997). DAs bind to DAF-12 and suppress its dauer-promoting activity (Antebi et al., 1998; Antebi et al., 2000). DAF-16 and DAF-12 stimulate each other but also have their own downstream programs (Gems et al., 1998; Matyash et al., 2004). The interplay between these factors determines whether worms enter diapause: when both are activated, dauer formation is induced. Although many transcriptional, as well as metabolic targets, of DAF-16 and DAF-12 have been elucidated in the context of diapause and longevity (Chen et al., 2015; Depuydt et al., 2014; Fisher and Lithgow, 2006; Fuchs et al., 2010; Hibshman et al., 2017; Holt and Riddle, 2003; Madi et al., 2008; Murphy et al., 2003; Seo et al., 2018; Wang and Kim, 2003), fundamental questions remain about the specific effectors of these pathways and how they interact to control the mode of metabolism required for quiescence on the one hand and growth on the other.

Here, we show that during dauer formation, the insulin pathway reduces global catabolism and energy expenditure by stimulating AMP-activated protein kinase (AMPK). FoxO-stimulated AMPK activity has a dual effect. On the one hand, it maintains low catabolism and high TOR pathway activity, while on the other, it acts together with the steroid hormone pathway to inhibit the TCA cycle and promote gluconeogenesis, thereby functioning as a metabolic turnout. Simultaneous inactivation of both these pathways leads to a switch from gluconeogenesis to an

bioRxiv preprint doi: https://doi.org/10.1101/323956; this version posted May 16, 2018. The copyright holder for this preprint (which was not certified by peer review) is the author/funder. All rights reserved. No reuse allowed without permission.

active TCA cycle. Remarkably, this metabolic transition is a prerequisite for the entry of the organism into reproductive growth.

bioRxiv preprint doi: https://doi.org/10.1101/323956; this version posted May 16, 2018. The copyright holder for this preprint (which was not certified by peer review) is the author/funder. All rights reserved. No reuse allowed without permission.

Results

DAF-16 induces a switch to low metabolic rate

To determine the relative contributions of the insulin and steroid hormone receptor pathways in the metabolic switch and morphological rearrangements of dauer larvae, we analyzed mutant strains and conditions in which only one of these pathways was active. We took advantage of the fact that a large group of Daf-c alleles of *daf-2*, designated class II, cannot be rescued by Daf-d mutations in *daf-12* or addition of DA and the worms arrest at L3 stage (Gems et al., 1998; Motola et al., 2006; Riddle, 1988). Thus, we used a mutant strain *daf-2;daf-12* as a paradigm for inactivation of DAF-12 (**Figure 1B**). In some experiments, inhibition of DAF-12 dauer-promoting activity was achieved by addition of dafachronic acid (DA) to *daf-2* mutant worms (**Figure 1B**). In both conditions, the activity of DAF-16 is very high (Gems et al., 1998). For inactivation of DAF-16, we used *daf-16* mutants grown on 4-methylated sterols (*daf-16* on 4-MS) such as lophenol, which makes the production of DAs impossible (Matyash et al., 2004). Under these conditions, DAF-12 is highly active, whereas DAF-16 is absent and worms arrest as dauer-like animals (**Figure 1C**) (Matyash et al., 2004).

Heat production is a measure of metabolic activity, and it is well known that the dauer state is associated with substantially lower heat production compared to that of other larval stages (Houthoofd et al., 2002). To understand which signaling pathways control metabolic activity, we measured heat production using time-resolved isothermal microcalorimetry. First, we compared the amounts of dissipated heat per unit time (heat flow) produced by larvae in reproductive development or undergoing dauer formation. Dauer formation was induced by substitution of dietary cholesterol in wild-type worms with 4-MS. Heat flow of synchronized L1 larvae was

bioRxiv preprint doi: https://doi.org/10.1101/323956; this version posted May 16, 2018. The copyright holder for this preprint (which was not certified by peer review) is the author/funder. All rights reserved. No reuse allowed without permission.

measured for 100 hours (**Figure 1D**). After a period of stabilization, heat flow increased both in larvae committed to dauer formation (on 4-MS) and in those committed to reproduction (on cholesterol). After about 24 hours, however, the two heat flow trends diverged (**Figure 1D**). Whereas larvae undergoing reproductive development continued increasing their heat production until they formed adults (50 hours), those undergoing dauer formation reached peak heat flow at 24 hours, and from that point on, they produced less and less heat (**Figure 1D**). Thus, dauer formation is associated with much lower heat production compared to that associated with reproductive development. Similar results were obtained with the Daf-c mutant *daf-7(e1372)*, which forms dauer larvae at the restrictive temperature of 25˚C but reproduces when DA is added (**Supplementary Figure 1**) (Motola et al., 2006).

Next, we investigated heat production in mutants with an active insulin pathway but with an inactivated steroid hormone pathway. For this, we compared a strain bearing the class II allele *daf-2(e1370)* with double mutant *daf-2(e1370);daf-12(rh61rh411)* larvae. Both strains reproduce at the permissive temperature of 15˚C but form dauers or arrest in L3 stage at the restrictive temperature of 25˚C (Gems et al., 1998). Heat flow at 25˚C displayed a very similar pattern in both cases: a shift to low metabolic activity after 24 hours (**Figure 1E**). Feeding *daf-2* with DA showed similar results (**Supplementary Figure 1**). Thus, DAF-12 is not required for the metabolic switch. In contrast, a double *daf-2(e1370);daf-16(mu86)* mutant that undergoes reproductive development at 25˚C (Gems et al., 1998) displayed high heat production similar to wild-type animals on cholesterol and *daf-7* on DA (**Figure 1E**). Together, these results indicate that decreased insulin signaling and, thus, activation of DAF-16 alone mediates the switch to low metabolic activity during dauer formation.

bioRxiv preprint doi: https://doi.org/10.1101/323956; this version posted May 16, 2018. The copyright holder for this preprint (which was not certified by peer review) is the author/funder. All rights reserved. No reuse allowed without permission.

DAF-12 controls dauer morphogenesis

Next, we asked whether DAF-16 or DAF-12 may determine the morphology of dauer larvae and whether metabolic state and morphology are interconnected. Our previous studies indicated that the activation of DAF-12 is important for dauer morphogenesis, because *daf-16* on 4-MS displayed some features of dauer morphology: radially constricted body and dauer-specific features of the cuticle such as alae and a striated layer (Matyash et al., 2004). To test this directly, we performed electron microscopy on *daf-2;daf-12* and *daf-2* larvae treated with DA and grown at the restrictive temperature of 25˚C, and compared them to L3 and dauer larvae. L3 larvae displayed a large body diameter, an elongated gut lumen with long, densely packed microvilli, and lack of dauer-specific cuticular structures such as alae and a striated layer (**Figure 2A**) (Albert and Riddle, 1988; Cassada and Russell, 1975). In addition, very few lipid droplets (LDs) could be observed (**Figure 2A**). In contrast, dauers had a typical radially constricted body and rounded gut lumen with very short microvilli. The cuticle possessed alae and a striated layer (**Figure 2B**) (Penkov et al., 2010). LDs were also numerous in many cells (**Figure 2B**). Interestingly, neither *daf-2;daf-12* nor *daf-2* on DA displayed any of the typical structural characteristics of dauers. Instead, they were reminiscent of L3 larvae (**Figure 2C** and **Supplementary Figure 2**). However, unlike L3 larvae and similar to dauers, *daf-2;daf-12* and DA-fed *daf-2* animals showed deposition of numerous LDs (**Figure 2C** and **Supplementary Figure 2**). Thus, DAF-12 controls dauer morphogenesis, whereas DAF-16 has no influence on this process but appears to affect metabolic changes that culminate in LD accumulation.

bioRxiv preprint doi: https://doi.org/10.1101/323956; this version posted May 16, 2018. The copyright holder for this preprint (which was not certified by peer review) is the author/funder. All rights reserved. No reuse allowed without permission.

Inactivation of DAF-16 causes uncontrolled catabolism and premature death of dauer larvae

Cells produce heat almost exclusively in catabolic reactions (Kemp and Guan, 1997). Thus, low heat production in dauers indicated that they have decreased catabolism and restricted energy expenditure. To determine which pathways regulate this process**,** we compared the cumulative heat output of *daf-2* dauers and *daf-2;daf-12* larvae for about 90 hours after they had completed the developmental arrest. Food was omitted to exclude any possible heat generation by bacterial cells. As seen in **Figure 3A**, *daf-2* dauers and *daf-2;daf-12* larvae produce very similar amounts of heat, showing that DAF-12 has no influence on the process. We next asked how loss of DAF-16 activity in the background of active DAF-12 would influence the metabolic rate. Compared to the wild-type dauers grown on 4-MS, *daf-16* animals cultivated in MS displayed around 1.43 fold higher heat production (**Figure 3B**). Together, these data suggest that DAF-16 suppresses catabolism/metabolic rate of dauers.

Catabolic reactions in dauers primarily use internal energy stores such as lipids, sugars and amino acids. We therefore monitored the breakdown of these molecules in *daf-2;daf-12* (active DAF-16) and *daf-16* on 4-MS (inactive DAF-16). Food was again omitted and thus only the catabolism of internal storage molecules was accounted for. Lipid levels were determined by Coherent Anti-Stokes Raman Scattering (CARS) microscopy (Camp Jr and Cicerone, 2015). This optical nonlinear technique allows label-free, noninvasive imaging of LDs, and can be used in live larvae (Jungst et al., 2011). *daf-2* dauers and *daf-2;daf-12* arrested larvae efficiently conserved their LDs, the main depot for storage lipids, over time (**Figure 3C**). Similar conservation of LDs was observed in wild-type dauers on 4-MS (**Figure 3C**). In contrast, *daf-16* dauers on 4-MS were almost entirely depleted of LDs even after two

bioRxiv preprint doi: https://doi.org/10.1101/323956; this version posted May 16, 2018. The copyright holder for this preprint (which was not certified by peer review) is the author/funder. All rights reserved. No reuse allowed without permission.

days in arrest (**Figure 3C**). Because LDs consist mainly of storage triglycerides (TGs), we also visualized worm lipids by thin-layer chromatography (TLC). Indeed, *daf-2* and 4-MS-treated wild-type dauers, as well as *daf-2;daf-12* larvae, showed a slow reduction of TG levels, whereas in *daf-16* on 4-MS, TGs were rapidly depleted and after two days only traces of them were observable (**Supplementary Figure 3A**). In contrast, the major membrane phospholipids were preserved in all animals over time, suggesting that no major degradation of membranes occurs (**Supplementary Figure 3A**). Thus, inactivation of DAF-16 induces fast depletion of TGs. TLC analysis further showed that sugars such as glucose and trehalose, and a variety of amino acids, are maintained at high levels in wild-type 4-MS dauers, *daf-2* and *daf-2;daf-12* larvae. In contrast, *daf-16* 4-MS larvae had only residual amounts of them after two days (**Supplementary Figure 3A** and **3B**). These results show that, in the absence of DAF-16, catabolism is not controlled and energy stores are dramatically depleted.

The above findings suggest that faster depletion of energy reserves might reduce survival in *daf-16* dauer-like larvae. Indeed, these animals deteriorate rapidly and perish after 12 days, whereas almost 100% of dauers and *daf-2;daf-12* arrested larvae were alive at the same time point (**Figure 3D**). Thus, DAF-16 regulates the survival of dauer larvae by controlling energy expenditure.

Inactivation of AAK-2 phenocopies the uncontrolled catabolism of *daf-16* mutants

The uncontrolled catabolism and mortality in *daf-16* on 4-MS were very similar to that observed in worms with defective AMPK signaling (Narbonne and Roy, 2009). It has been shown previously that loss of activity of the AMPK α-subunit homolog

bioRxiv preprint doi: https://doi.org/10.1101/323956; this version posted May 16, 2018. The copyright holder for this preprint (which was not certified by peer review) is the author/funder. All rights reserved. No reuse allowed without permission.

AAK-2 results in early dauer lethality attributed to loss of lipid deposits (Narbonne and Roy, 2009), suggesting that DAF-16 and AAK-2 may have overlapping functions or act jointly by controlling dauer energy expenditure. To test whether *aak-2* mutant dauers also display rapid loss of TGs, sugars and amino acids, we generated a *daf-2(e1370);aak-2(gt33)* strain that harbors a large deletion in *aak-2*. At the restrictive temperature of 25˚C, almost all animals formed dauer larvae. They showed very high survival after treatment with the detergent SDS characteristic only for dauers (**Figure S4A** and **B**) (Albert and Riddle, 1983). Also, as shown by electron microscopy, these larvae displayed typical dauer features, including radial constriction of the body, alae and striated layer of the cuticle (**Figure 4A**). In a previous study using a similar strain, *daf-2(e1370);aak-2(ok524)*, bearing a different deletion in *aak-2*, it was shown that at 25˚C the animals undergo dauer formation but spontaneously exit from dauer state and eventually produce adult animals within five days (Cunningham et al., 2014). To test whether our mutant would behave similarly, we incubated the *daf-2(e1370);aak-2(gt33)* dauers on solid medium with ample food source for five days at 25˚C. We did not detect spontaneous exit from dauer state within this period, and the worms displayed almost 100% survival in SDS (**Supplementary Figure 4A** and **B**). The dauer-specific alae and striated layer of the cuticle were also observable by electron microscopy (**Figure 4A**). These data indicated that *daf-2(e1370);aak-2(gt33)* was very suitable model to study the rationing of energy reserves in dauer state. The dissimilarity between our observations and the data published in the study mentioned above (Cunningham et al., 2014) could be explained with the use of different growth media and alleles of *aak-2*, as well as with differences in the genetic background. Importantly, the electron micrograms of *daf-2;aak-2* dauers suggested that after five days they enter a state similar to starvation as judged by an extreme decrease of the

bioRxiv preprint doi: https://doi.org/10.1101/323956; this version posted May 16, 2018. The copyright holder for this preprint (which was not certified by peer review) is the author/funder. All rights reserved. No reuse allowed without permission.

cellular volume of the hypodermis, expansion of the body cavities and deterioration of the mitochondrial network (**Figure 4A**). Lipid droplets were also not observable (**Figure 4A**). This again pointed out to the possibility that AAK-2 is required for the preservation of the energy reserves. Indeed, in *daf-2;aak-2(gt33)* there was a rapid depletion of TGs and trehalose (**Figure 4B** and **C**), as well as amino acids (**Supplementary Figure 5A and 5B**), similar to that observed in *daf-16* on 4-MS. Phosphatidylethanolamines were unaffected (**Figure 4B** and **C**), indicating a lack of change in phospholipid content. Thus, *daf-16* and *aak-2* have highly related phenotypes in terms of catabolism in dauer state, suggesting that they might act in the same pathway.

DAF-16 prevents TOR-pathway dependent starvation response and this requires intact AAK-2

The severe depletion of energy reserves in *daf-2;aak-2* dauer larvae suggests that they enter a state similar to starvation. One of the hallmarks of the cellular response to starvation is decreased TOR pathway activity (Sheaffer et al., 2008; Wullschleger et al., 2006). To determine whether the absence of AAK-2 induces a starvation-like response, we therefore monitored TOR activity using a strain expressing the small nucleolar ribonucleoprotein (snoRNP) FIB-1 tagged with eGFP. It is known that FIB-1 is localized to the nucleolus in worms with an active TOR pathway, whereas the nucleolar localization of FIB-1 is greatly reduced in response to starvation or loss of TOR activity (Sheaffer et al., 2008). Wild-type dauers had nucleolar FIB-1 localization similar to that of well-fed, reproductive larva, despite the lack of nutrition from the environment (**Supplementary Figure 6A**). Thus, with sufficient energy reserves, dauers do not display a TOR-dependent starvation response. Following

bioRxiv preprint doi: https://doi.org/10.1101/323956; this version posted May 16, 2018. The copyright holder for this preprint (which was not certified by peer review) is the author/funder. All rights reserved. No reuse allowed without permission.

arrest in *daf-2* and *daf-2;aak-2* dauers, as well as in *daf-2* DA-fed arrested L3 larvae, there was an initial period in which all animals displayed nucleolar FIB-1 (**Figure 5A, B and C**). This localization remained unchanged over time in *daf-2* dauers and *daf-2* DA-fed arrested L3 larvae, suggesting that activation of DAF-16 is sufficient to maintain the nucleolar localization of FIB-1 over time and this process does not require active DAF-12 (**Figure 4A and B**). In *daf-2;aak-2* dauers, however, FIB-1 formed granular, punctate structures in the nucleoplasm of cells (**Figure 4C**) 4 days after arrest. Furthermore, after 7 days, FIB-1 was almost completely dispersed in the nucleoplasm of almost all cells (**Figure 4C**). Thus, DAF-16 could prevent a TOR-dependent starvation response only in the presence of an intact AAK-2.

DAF-16 and DAF-12 control the transition from TCA cycle to gluconeogenesis independently

Dauers undergo a shift from TCA cycle to gluconeogenesis, accumulating large amounts of the disaccharide trehalose and reducing their oxygen consumption to about 20% (Erkut et al., 2016). To determine whether DAF-16 or DAF-12 is responsible for this transition, we used our previously developed 2D-TLC method to trace the metabolism of radiolabeled acetate (Erkut et al., 2016). Using this approach, it is possible to distinguish clearly between the gluconeogenic mode and the TCA mode because the radiolabeled carbon derived from acetate can only be incorporated into sugars if the glyoxylate shunt and the gluconeogenesis are active (Erkut et al., 2016). First, we grew *daf-2* and *daf-2;daf-12* animals on food containing ^{14}C-acetate at permissive (15˚C) or restrictive (25˚C) temperature. At 15˚C, the reproductive L3 larvae of both strains distributed the acetate label between various metabolites, including amino acids and sugars (**Figure 6A**). However, the sugars (trehalose and

bioRxiv preprint doi: https://doi.org/10.1101/323956; this version posted May 16, 2018. The copyright holder for this preprint (which was not certified by peer review) is the author/funder. All rights reserved. No reuse allowed without permission.

glucose) were not strongly labelled, indicating that the TCA cycle is prevalent. In accordance with our previous study (Erkut et al., 2016), at 25˚C the *daf-2* dauers displayed strong accumulation of acetate-labelled trehalose, indicating a switch to intensive glyoxylate shunt and gluconeogenesis (**Figure 6A**). Extensive incorporation of acetate into trehalose was also observed in *daf-2;daf-12* arrested L3 larvae (**Figure 6A**). Thus, activation of DAF-16 triggers a switch from TCA cycle to gluconeogenesis in the absence of DAF-12.

We next asked whether DAF-12 has a role in the switch from TCA to gluconeogenesis. In a similar experiment, we labelled wild-type and *daf-16* worms on cholesterol or 4-MS with ^{14}C-acetate. The TLC patterns of animals grown on cholesterol were consistent with an active TCA cycle (**Figure 6B**). As expected, 4-MS treated wild-type dauers displayed gluconeogenic mode (**Figure 6B**). To our surprise, however, extensive accumulation of acetate into trehalose was also observed in *daf-16* on 4-MS (**Figure 6B**). This shows that activation of DAF-12 can trigger a switch towards a gluconeogenic mode in the absence of DAF-16. It also demonstrates that low energy expenditure and the gluconeogenic mode can be uncoupled under conditions of low DAF-16 but high DAF-12 activity.

AAK-2 and DAF-12 together control the transition between growth and quiescence

As shown above, DAF-16 activity limits the energy expenditure of dauer larvae and induces a switch from TCA cycle to gluconeogenesis. Since *aak-2* abolished the reduction of energy expenditure in *daf-2* dauers, we asked whether it could also abolish the gluconeogenic mode in these animals. To test this, we performed ^{14}C-acetate labelling of *daf-2;aak*-2 grown at permissive (15˚C) or at restrictive (25˚C)

bioRxiv preprint doi: https://doi.org/10.1101/323956; this version posted May 16, 2018. The copyright holder for this preprint (which was not certified by peer review) is the author/funder. All rights reserved. No reuse allowed without permission.

temperature. As expected, at 15˚C the worms showed a metabolic pattern characteristic of an active TCA cycle (**Figure 7A**). At 25˚C, *daf-2;aak-2* dauers displayed a pronounced gluconeogenic mode (**Figure 7A**). To test whether this pattern was due to DAF-12 activity, we inhibited DAF-12 in *daf-2;aak-2* by adding DA. Remarkably, under these conditions the gluconeogenic mode was completely abolished (**Figure 7A**). Thus, loss of *aak-2* suppresses both the switch to low energy expenditure and to gluconeogenesis induced by DAF-16.

The above results show that the metabolic transition induced by DAF-16 requires intact AAK-2. Combined with the report that a strain *daf-2(e1370);aak-2(ok524)* has increased exit from dauer state (Cunningham et al., 2014), this suggests that the metabolic transition is associated with growth arrest. To test this possibility, we monitored the growth of *daf-2* and *daf-2;aak-2* worms at 25˚C on food supplemented with DA. Astoundingly, unlike *daf-2*, the *daf-2;aak-2* animals did not arrest and almost all animals developed into adults, completely bypassing dauer arrest (**Figure 7B** and **C**). In addition, they showed nucleolar FIB-1 localization consistent with active TOR signaling (**Supplementary Figure 6B**). Thus, DAF-16/AAK-2 and DAF-12 control the transition from growth to quiescence by governing the metabolic switch.

bioRxiv preprint doi: https://doi.org/10.1101/323956; this version posted May 16, 2018. The copyright holder for this preprint (which was not certified by peer review) is the author/funder. All rights reserved. No reuse allowed without permission.

Discussion

The results presented in this study demonstrate that the global metabolic transition observed in dauer larva is regulated by the concerted action of the insulin, steroid hormone receptor and AMPK pathways. Most importantly, the insulin, AMPK and steroid hormone pathways serve as metabolic turnouts by decreasing TCA cycle activity and activating gluconeogenesis. The transition between growth and quiescence (or vice versa) depends directly on this metabolic switch. We also show that metabolic mode and morphology are independently regulated, since the arrested larvae of *daf-2;daf-12* mutants display dauer metabolism but reproductive morphology.

Our results provide insights into how major signaling pathways govern the metabolic transition. Under conditions that favor reproductive growth (**Fig. 7A**), various insulin-like peptides, responding to environmental and internal stimuli, activate DAF-2, leading to inhibition of DAF-16 and, downstream or in parallel to it, of AAK-2. Meanwhile, the TGF-β and the guanylyl cyclase pathways, which are active in the absence of dauer-inducing pheromones, stimulate the production of DAs by DAF-9, resulting in inhibition of DAF-12. Due to the down-regulation of AAK-2 and DAF-12, the TCA cycle is activated, whereas gluconeogenesis and the expression of dauer-specific genes (e.g. genes required for dauer morphogenesis) are inhibited. The TCA cycle powers global anabolism by providing energy from OXPHOS and building blocks for biosynthetic reactions. At the same time, the low activity of AAK-2 enables high catabolic activity which supports anabolism by streaming carbon and energy obtained from nutrients into it. In this manner, enough energy, reducing equivalents and building blocks are produced for growth and reproduction.

bioRxiv preprint doi: https://doi.org/10.1101/323956; this version posted May 16, 2018. The copyright holder for this preprint (which was not certified by peer review) is the author/funder. All rights reserved. No reuse allowed without permission.

Under conditions that favor dauer formation, metabolic status is very different (**Figure 7B**). The decrease in insulin ligands activates DAF-16 and AAK-2. Meanwhile, the TGF-β and guanylyl cyclase pathways are silent due to the abundance of pheromones, resulting in inhibition of DAF-9 and activation of DAF-12. AAK-2 and DAF-12 inhibit the TCA cycle and stimulate gluconeogenesis mainly from lipids. This favors the production of sugars for glycolysis and lowers OXPHOS and the production of building blocks for biosynthetic reactions. In this way, global anabolism is decreased. Meanwhile, AAK-2 inhibits catabolism, and this prevents excessive degradation of internal energy reserves. Thus, building blocks and energy for anabolism are not produced and the energy expenditure is kept low. Consequently, worms enter a long-lasting dauer state.

The metabolic switch that occurs during dauer formation must be coordinated with the developmental timing. During growth arrest, cells must simultaneously undergo metabolic depression and acquire dauer-specific fates. Therefore, the master regulators of dauer formation, DAF-12 and DAF-16, should also regulate cell fate decisions. Indeed, DAF-12 has been shown to suppress the progression through larval stages and to determine the cell fates via microRNAs of the *let-7* family (Antebi, 2013b), suggesting that it functions as both a metabolic and a developmental "turnout". Similarly, it has been demonstrated that the insulin (via the PTEN homolog DAF-18) and AMPK signaling cascades are crucial for the arrest of the germline cell proliferation during dauer formation (Narbonne and Roy, 2006). Thus, the investigation of how the synchronization of the metabolic and the developmental programs is achieved will be an important subject for future studies.

Our finding that AMPK modulates the effect of insulin pathway signaling in the control of metabolic mode and growth resolves a long-standing problem in the

bioRxiv preprint doi: https://doi.org/10.1101/323956; this version posted May 16, 2018. The copyright holder for this preprint (which was not certified by peer review) is the author/funder. All rights reserved. No reuse allowed without permission.

field. Since class II *daf-2* alleles cannot be rescued by *daf-12* Daf-d mutations or addition of DA (Gems et al., 1998; Motola et al., 2006), it was postulated that an unknown factor mediates larval arrest in worms with active DAF-16 but inactive DAF-12 (Gems et al., 1998). Our data indicate that this factor is AAK-2, which shows that the AMPK signaling has much broader impact on dauer metabolism than previously reported. In addition to the known effects of the AMPK on the regulation of lipid reserves, lipolysis, and lipid droplet localization (Narbonne and Roy, 2009; Xie and Roy, 2012, 2015a, b), we provide evidence that in dauers it also determines the activities of the core metabolic pathways: TCA cycle, gluconeogenesis, glycolysis, and amino acid catabolism. In agreement with our observations, AMPK has been described in *C. elegans* as a modulator of the energy metabolism and mitochondrial function in the responses to various kinds of metabolic stress (Burkewitz et al., 2015; Moreno-Arriola et al., 2016; Moroz et al., 2014; Possik et al., 2015; Weir et al., 2017; Zarse et al., 2012). Since energy production is essential for the execution of developmental transcriptional programs, developing organisms must be able to respond to changes in cellular energetic status. AMPK is an established sensor of AMP levels in the cell and, thus, might integrate insulin signaling with the energetic status. This notion is consistent with the work of other groups, showing that AMPK acts at least partially downstream of DAF-16 (Tullet et al., 2014) and *aak-2* loss-of-function alleles suppress the extension of adult life span in *daf-2* mutants (Apfeld et al., 2004).

Our work in dauer larvae may provide important insights into the regulation of metabolic switches. It seems likely, for instance, that the coordination between energy metabolism and growth observed in this study is conserved in other developmentally arrested stages such as the L1 diapause and the adult reproductive diapause that

bioRxiv preprint doi: https://doi.org/10.1101/323956; this version posted May 16, 2018. The copyright holder for this preprint (which was not certified by peer review) is the author/funder. All rights reserved. No reuse allowed without permission.

protect *C. elegans* during starvation periods (Angelo and Van Gilst, 2009; Kaplan et al., 2015). Since these stages are widely used as models of the starvation response in higher animals, we might predict that the interaction between the insulin, AMPK and steroid hormone pathways might also coordinate growth and metabolism during starvation in these organisms as well. Dauer metabolism is also highly reminiscent of Warburg metabolism in cancer cells, which is characterized by predominantly aerobic glycolysis and decreased OXPHOS. Thus, the transition from reproductive growth to the dauer state could provide a model of transformation to cancer metabolism in mammalian cells. Remarkably, in contrast to cancer cells, dauer cells do not proliferate, suggesting that Warburg metabolism may be regulated independently of malignant growth. One of the major issues to be solved in the future will be to clarify how the TCA cycle is switched to gluconeogenesis. Probably it is not a simple binary switch but a multicomponent system, involving the regulation of many enzymes. It is possible that suppression of the TCA cycle alone could not produce this effect. Indeed, it was recently shown that treatment of worms with the TCA cycle inhibitor arsenite induces a Warburg-like metabolic state (Luz et al., 2016). However, under these conditions no evidence for gluconeogenesis was provided.

For several decades, the *C. elegans* insulin/AMPK and steroid hormone pathways have been studied intensively because of their association with post-reproductive lifespan extension and diapause (Antebi, 2013a; Hand et al., 2016; Martins et al., 2016). Here, we have shown that these pathways are major regulators of the metabolic switch. These results suggest that most probably not only the diapause but also the lifespan extension will be ultimately connected to the combined regulation of metabolic rates and growth, thus highlighting the intricate relationship between growth, development, aging and metabolic state.

bioRxiv preprint doi: https://doi.org/10.1101/323956; this version posted May 16, 2018. The copyright holder for this preprint (which was not certified by peer review) is the author/funder. All rights reserved. No reuse allowed without permission.

Author contributions

S.P., C.E., J.-M.V., E.K. K.F. and T.V.K. designed the experiments. S.P. conducted phenotypical, fluorescent microscopy and biochemical experiments. S.P., C.E. and J.O. performed microcalorimetry experiments. R.G. optimized and performed CARS microscopy. D.V. obtained electron microscopy images. S.P., C.E., J.O., R.G., D.V., and T.V.K. analyzed the data. All authors discussed the results and S.P. and T.V.K. wrote the manuscript.

bioRxiv preprint doi: https://doi.org/10.1101/323956; this version posted May 16, 2018. The copyright holder for this preprint (which was not certified by peer review) is the author/funder. All rights reserved. No reuse allowed without permission.

Acknowledgments

We thank all members of Kurzchalia lab for helpful discussions, Prof. Richard Roy (McGill University, Montreal, Quebec, Canada) for critically reading the manuscript, and Dr. Iain Patten for the writing support. We are grateful to the Caenorhabditis Genetics Center and to Prof. Adam Antebi (Max Planck Institute for Biology of Ageing, Cologne, Germany) for providing worm strains. We thank Prof. Hans-Joachim Knölker (TU Dresden, Germany) for the synthesis of lophanol and dafachronic acid.

bioRxiv preprint doi: https://doi.org/10.1101/323956; this version posted May 16, 2018. The copyright holder for this preprint (which was not certified by peer review) is the author/funder. All rights reserved. No reuse allowed without permission.

Methods

Material and *C. elegans* strains

Lophenol was purchased from Research Plus (Manasquan, NJ USA), [1-^{14}C]-acetate (sodium salt) from Hartmann Analytic (Braunschweig, Germany), and Dulbecco's medium (DMEM) from Invitrogen (Karlsruhe, Germany). (25*S*)-Δ^{7}–DA and lophanol were produced in the Laboratory of Prof. H.-J. Knölker. All other chemicals were from Sigma-Aldrich (Taufkirchen, Germany).

The Caenorhabditis Genetics Centre (CGC) provided the following *C. elegans* strains: N2 (Bristol strain), *daf-7(e1372), daf-2(e1370), daf-16(mu86), aak-2(gt33), unc-119(ed3);knuSi221*. The strain *unc-119(ed3);knuSi221* contains a single-copy transgenic segment *fib-1*p::*fib-1*(genomic)::eGFP::*fib-1* 3' UTR + *unc-119*(+). The *E. coli* strain NA22 was also provided by the CGC.

The compound mutant and transgenic strains *daf-2(e1370);daf-12(rh61rh411), daf-16(mu86);daf-2(e1370), daf-2(e1370);aak-2(gt33), daf-2(e1370);knuSi221* (abbreviated *daf-2;fib-1::eGFP*), *daf-2(e1370);aak-2(gt33);knuSi221* (abbreviated *daf-2;aak-2;fib-1::eGFP*) were generated during this or past studies as published or described below (Hannich et al., 2009; Matyash et al., 2004).

Generation of *daf-2;aak-2*

Heterozygous *daf-2(e1370)* males were crossed to *aak-2(gt33)* hermaphrodites. The resulting males were crossed back to the parental *aak-2(gt33)* worms. This gave rise to hermaphrodites that laid eggs at 25˚C. A fraction of these eggs developed into dauers. These dauers were shifted to 15˚C to re-enter reproductive growth, singled

bioRxiv preprint doi: https://doi.org/10.1101/323956; this version posted May 16, 2018. The copyright holder for this preprint (which was not certified by peer review) is the author/funder. All rights reserved. No reuse allowed without permission.

and genotyped by polymerase chain reaction (PCR) for the presence of the *aak-2(gt33)* deletion.

Generation of *daf-2;fib-1::eGFP* and *daf-2;aak-2;fib-1::eGFP*

Males of *unc-119(ed3);knuSi221* were crossed to hermaphrodites of *daf-2(e1370);aak-2(gt33)*. Hermaphrodites from the progeny laid eggs at 25˚C that developed into dauers. The dauers were left to recover at 15˚C and eGFP-positive worms were selected and singled. The progeny of these worms was selected based on fluorescent signal. The presence of *aak-2(gt33)* was tested by PCR and two types of strains were selected as final products of the cross: animals homozygous for the wild-type *aak-2* allele (*daf-2;fib-1::eGFP*) and animals homozygous for *aak-2(gt33)* (*daf-2;aak-2;fib-1::eGFP*).

Growth and radiolabeling of *C. elegans* strains

The worm strains were routinely propagated on NGM-agar plates complemented with *E. coli* NA22 (Brenner, 1974). When indicated, (25*S*)-Δ^{7}–DA was added to the bacteria to a 250 nM final concentration, calculated according to the volume of the NGM-agar. The temperature-sensitive dauer constitutive strains bearing *daf-7(e1372)* or *daf-2(e1370)* alleles were propagated at 15˚C, a temperature at which they undergo reproductive growth. To obtain dauers or arrested L3 larvae of these strains, embryos were obtained from gravid adults by hypochlorite treatment (Brenner, 1974), incubated overnight at room temperature, and the resulting synchronized L1 larvae were grown at 25˚C for 72 hours.

The growth on 4-MS-containing medium was performed according to a described method (Matyash et al., 2004). Briefly, sterol-depleted medium was

bioRxiv preprint doi: https://doi.org/10.1101/323956; this version posted May 16, 2018. The copyright holder for this preprint (which was not certified by peer review) is the author/funder. All rights reserved. No reuse allowed without permission.

obtained by substituting agar with chloroform-extracted agarose. NA22 bacteria were grown on a sterol-free DMEM medium, pelleted, rinsed and resuspended in M9 buffer. Two different 4-MS were used depending on the availability: lophenol or lophanol. It must be noted that these two compounds have identical effects to those of dietary sterols (Matyash et al., 2004). The 4-MS (or cholesterol, when indicated) were added to the bacteria to a 13 μM final concentration according to the volume of the agarose. The worms were propagated on these plates for two consecutive generations. Again, synchronized L1 larvae were grown at 25˚C for 72 hours in the second generation until the developmental arrest occurred.

For the microscopy of FIB-1::eGFP in a wild-type background, mixed populations were produced on NGM-agar plates as described above. Reproductive larvae were collected from plates with abundant food and low population density. Dauer larvae were prepared from overcrowded plates, and isolated from other stages by treatment with 1% SDS for 30 minutes followed by separation of the survived dauers from the dead debris of other stages on empty agarose plates on which the dauer larvae quickly dispersed.

To obtain radiolabeled *C. elegans*, the worms were grown on NGM-agar or agarose solid medium (see above), complemented with [1-^{14}C]-acetate (sodium salt). The ^{14}C-acetate was added to the bacteria and calculated as 0.5 μCi/ml according to the volume of the NGM-agar/agarose.

Survival, SDS assay and worm sampling for microscopy and biochemical analysis

Dauer(-like) and arrested L3 larvae were prepared by growing the worms on solid medium as described above, collected and washed three times with M9 buffer. The

bioRxiv preprint doi: https://doi.org/10.1101/323956; this version posted May 16, 2018. The copyright holder for this preprint (which was not certified by peer review) is the author/funder. All rights reserved. No reuse allowed without permission.

worms were incubated in 15 ml polypropylene centrifuge tubes (Corning, NY, USA) containing 10 ml of autoclaved M9 buffer supplemented with the antibiotics streptomycin (50 μg/ml) and nystatin (10 μg/ml) at 25˚C under constant agitation. The density of the population was kept at 500 worms/ml. To monitor the survival, 100 μl aliquots were taken every 2 days and the percentage of live animals was calculated. For scoring the survival of *daf-2* or *daf-2;aak-2* after SDS treatment, worms were collected from the feeding NGM-agar plates, washed three times with ddH_2O and resuspended in 10 ml of 1% SDS (w/v) in ddH_2O in 15 ml polypropylene centrifuge tubes (Corning, NY, USA). After 30 minutes of incubation within the SDS solution at 25˚C with shaking, the worms were washed another three times with ddH_2O and placed on NGM agar plates where the survival was scored.

100 μl aliquots were also used for the preparation of microscopy samples as described below. For biochemical analysis, the worms were washed three times with ddH_2O, pelleted, snap-frozen in liquid nitrogen and stored at -80˚C until further analysis (see below).

Isothermal microcalorimetry

To measure the heat production during worm development starting from L1 larva onwards, we first purified eggs and plated them on agarose plates without food. After keeping them at 25 ˚C overnight, synchronized L1 larvae were washed with M9 buffer and diluted to 14.3 worms/μl. 140 μl (~2000 worms) of each suspension was pipetted into a 4 ml glass ampoule (TA Instruments, New Castle, DE, USA), in which there was already 60 μl of concentrated *E. coli* NA22 in M9 (OD_{600} = 20), so that the starting amount of bacteria was 6 OD_{600}. These ampoules were then sealed with aluminium caps equipped with sealing discs (TA Instruments, New Castle, DE, USA).

bioRxiv preprint doi: https://doi.org/10.1101/323956; this version posted May 16, 2018. The copyright holder for this preprint (which was not certified by peer review) is the author/funder. All rights reserved. No reuse allowed without permission.

For the measurements of the heat production of dauer(-like) and arrested L3 larvae, worms were grown on solid medium as described above and washed three times with M9 buffer. 2000 larvae were collected in 200 μl of autoclaved M9 buffer supplemented with the antibiotics streptomycin (50 μg/ml) and nystatin (10 μg/ml) and transferred into 4 ml glass ampoules that were closed with aluminum caps equipped with sealing discs (TA Instruments, New Castle, DE, USA).

Isothermal calorimetric measurements were performed with a TAMIII (Thermal Activity Monitor) instrument (Waters GmbH, Eschborn, Germany) equipped with 12 microcalorimeters in twin configuration (one side for the sample the other for a steel reference) to continuously monitor the metabolic heat produced by *C. elegans* at 25°C for up to 5 days. The samples were held in the TAM III in a waiting position for 15 min before complete insertion followed by 45 min equilibration. In each experiment, thermograms were recorded at least in triplicates. The termograms represent continuous measurements and no curve fitting was performed.

Fluorescence and CARS microscopy

For the visualization of FIB-1::eGFP by confocal microscopy and for CARS imaging of lipid deposits, worms were mounted on 2% agarose pads on glass slides (Thermo scientific, Superfrost Plus,) and anesthetized with 20 mM sodium azide in M9 buffer. The liquid was aspirated and the pads were covered with cover slips (with 0.17 +/- 0.005 mm cover slips (Menzel-Glaeser,).

The FIB-1::eGFP was visualized with a Zeiss LSM 880 scanning confocal microscope equipped with a Zeiss i LCI Plan-Neofluar 63x 1.3 Imm Korr DIC objective. eGFP was excited at 488 nm, and fluorescence was detected at the emission band of 490-540 nm. On average, 12 optical sections of 0.09x0.09x1 μm voxel size

bioRxiv preprint doi: https://doi.org/10.1101/323956; this version posted May 16, 2018. The copyright holder for this preprint (which was not certified by peer review) is the author/funder. All rights reserved. No reuse allowed without permission.

were collected. To represent the status of the nucleoli in all tissues within the frame, all micrographs are represented as a maximum intensity projection of the Z-stack generated in Fiji.

The imaging of lipid droplets was performed by coherent anti-Stockes Raman scattering (CARS) microscopy. Autogenous two-photon excited fluorescence (TPEF) and second harmonic generation (SHG) optical signals were simultaneously acquired. TPEF was used to differentiate between lipid droplets and autofluorescent lysosome-related organelles (Hermann et al., 2005). SHG displays collagen type I and was used as reference for anatomical details, e.g. the position of the pharynx (Williams et al., 2005). CARS, TPEF and SHG were detected using a multiphoton scanning microscope coupled with two near-infrared picosecond fiber lasers. The optical microscope was an upright Axio Examiner Z.1 equipped with a laser scanning module LSM 7 (all from Carl Zeiss Microscopy GmbH, Jena, Germany) and multiple detectors in non-descanned configuration. The excitation for TPEF and SHG was provided by an Erbium fiber laser (Femto Fiber pro NIR from Toptica Photonics AG, Gräfelfing, Germany) emitting at 781 nm with pulse length of 1.2 ps and maximum emitted power at the source of 100 mW. The TPEF signal in the spectral range 500-550 nm was acquired in reflection. The SHG signal was acquired in transmission mode with band pass (BP) filter (390 ± 9) nm. A second laser source was used to excite the CARS signal. This source (Femto Fiber pro TNIR from Toptica Photonics AG) is tunable in the range 850 - 1100 nm and has a pulse length of 0.8 ps. In all CARS experiments the wavelength was set to 1005 nm (emitted power at the source:1.5 mW), to resonantly excite the symmetric stretching vibration of methylene groups at 2850 cm^{-1}. The CARS signal was collected in transmission mode and selected using a BP filter (640 ± 7) nm. A water immersion objective W Plan-

bioRxiv preprint doi: https://doi.org/10.1101/323956; this version posted May 16, 2018. The copyright holder for this preprint (which was not certified by peer review) is the author/funder. All rights reserved. No reuse allowed without permission.

Apochromat 20×/1.0 (Carl Zeiss Microscopy GmbH) was used. Due to the transmission of optical elements, the laser power in the sample was 52 mW. CARS, TPEF and SHG were combined as RGB images (red: CARS; green: TPEF; blue: SHG). An automatic tiling procedure enabled by the microscope software ZEN was used for acquisition of images larger than the field of view of the microscope objective.

High-pressure freezing and electron microscopy

Worms were directly frozen without any additives with a high-pressure freezing unit (EMPACT2, Leica), followed by automated freeze substitution (AFS2, Leica) in acetone cocktail (containing 1% osmium tetroxide, 0.1% uranyl acetate and 0.5% glutaraldehyde), with a slope of 3.0ºC/hour, from -90ºC up to 0ºC (including a rest for 15 hours at -30ºC). At room temperature, samples were rinsed with acetone and stepwise infiltrated with mixtures of acetone and LX112-resin (Ladd Research) from 1/3 over ½ to 2/3 the amount of resin (1.5 hours each step). Samples were left in pure resin overnight, then for another four hours in fresh resin before mounting them between slides and polymerizing at 60ºC. Transverse sections (70 nm) were taken with an ultramicrotome (Ultracut UCT, Leica), and post-contrasted in 1% uranyl acetate in 70% methanol followed by lead citrate. The sections were examined under electron microscope (Philips Tecnai12, FEI) at 120 kV, and photographs were taken with a TVIPS-camera (Tietz).

Organic extraction and thin layer chromatography

Frozen worm pellets were homogenized by three rounds of thawing in an ultrasonication bath and freezing, and extracted using a standard method (Bligh and

bioRxiv preprint doi: https://doi.org/10.1101/323956; this version posted May 16, 2018. The copyright holder for this preprint (which was not certified by peer review) is the author/funder. All rights reserved. No reuse allowed without permission.

Dyer, 1957). In all experiments, the samples consisted of similar numbers of worms (~20 000 larvae). After phase separation, lipids and hydrophilic metabolites were recovered from the organic and aqueous phases, respectively. Non-radioactive samples were normalized for the number of worms. Radioactive ^{14}C-acetate-labeled samples were normalized for the number of worms to visualize the rate of catabolism of TGs, phospholipids, trehalose and amino acids in *daf-2;aak-2* (**Fig. 4A** and **B** and **Fig. S4**) or according to the total radioactivity to determine the state of the gluconeogenesis in different worms strains (**Fig. 5A and B** and **6A**). In the latter case, the normalization method was chosen to obtain information on the relative abundance of the various metabolites.

TLC was performed on 10 cm HPTLC plates (Merck, Darmstadt, Germany). The running system for sugar detection was chloroform-methanol-water (4:4:1, v/v/v) and chloroform-methanol-water (45:18:3, v/v/v) for phospholipid detection. 2D-TLC for the visualization of hydrophilic metabolites was done using 1-propanol–methanol–ammonia (32%)–water (28:8:7:7, v/v/v/v) as 1st system and 1-butanol–acetone–glacial acetic acid–water (35:35:7:23, v/v/v/v) as the 2nd. The TLC plates were sprayed with Molisch reagent for sugar detection, with ninhydrin for visualization of amino acid, and with 3% copper (II) acetate in 10% orthophosphoric acid for imaging of TGs and phospholipids. TLC plates containing radioactive samples were sprayed with EN^{3}HANCE spray surface autoradiography enhancer (Perkin Elmer, Waltham, MA, USA) and exposed to X-ray film (Kodak Biomax MR, Sigma-Aldrich, Taufkirchen, Germany). The X-ray films were scanned and the band intensities of TGs, phosphatidylethanolamines and trehalose were calculated in Fiji by determining the corresponding optical density peak areas.

bioRxiv preprint doi: https://doi.org/10.1101/323956; this version posted May 16, 2018. The copyright holder for this preprint (which was not certified by peer review) is the author/funder. All rights reserved. No reuse allowed without permission.

References

Albert, P.S., and Riddle, D.L. (1983). Developmental alterations in sensory neuroanatomy of the Caenorhabditis elegans dauer larva. J Comp Neurol *219*, 461-481.

Albert, P.S., and Riddle, D.L. (1988). Mutants of Caenorhabditis elegans that form dauer-like larvae. Dev Biol *126*, 270-293.

Angelo, G., and Van Gilst, M.R. (2009). Starvation protects germline stem cells and extends reproductive longevity in C. elegans. Science *326*, 954-958.

Antebi, A. (2013a). Regulation of longevity by the reproductive system. Exp Gerontol *48*, 596-602.

Antebi, A. (2013b). Steroid regulation of C. elegans diapause, developmental timing, and longevity. Curr Top Dev Biol *105*, 181-212.

Antebi, A., Culotti, J.G., and Hedgecock, E.M. (1998). daf-12 regulates developmental age and the dauer alternative in Caenorhabditis elegans. Development *125*, 1191-1205.

Antebi, A., Yeh, W.H., Tait, D., Hedgecock, E.M., and Riddle, D.L. (2000). daf-12 encodes a nuclear receptor that regulates the dauer diapause and developmental age in C. elegans. Genes Dev *14*, 1512-1527.

Apfeld, J., O'Connor, G., McDonagh, T., DiStefano, P.S., and Curtis, R. (2004). The AMP-activated protein kinase AAK-2 links energy levels and insulin-like signals to lifespan in C. elegans. Genes Dev *18*, 3004-3009.

Bligh, E.G., and Dyer, W.J. (1957). A rapid method of total lipid extraction and purification. Can J Biochem Physiol *37*, 911-917.

Brenner, S. (1974). The genetics of Caenorhabditis elegans. Genetics *77*, 71-94.

bioRxiv preprint doi: https://doi.org/10.1101/323956; this version posted May 16, 2018. The copyright holder for this preprint (which was not certified by peer review) is the author/funder. All rights reserved. No reuse allowed without permission.

Burkewitz, K., Morantte, I., Weir, H.J.M., Yeo, R., Zhang, Y., Huynh, F.K., Ilkayeva, O.R., Hirschey, M.D., Grant, A.R., and Mair, W.B. (2015). Neuronal CRTC-1 governs systemic mitochondrial metabolism and lifespan via a catecholamine signal. Cell *160*, 842-855.

Burnell, A.M., Houthoofd, K., O'Hanlon, K., and Vanfleteren, J.R. (2005). Alternate metabolism during the dauer stage of the nematode Caenorhabditis elegans. Exp Gerontol *40*, 850-856.

Butcher, R.A. (2017). Small-molecule pheromones and hormones controlling nematode development. Nature chemical biology *13*, 577-586.

Cairns, R.A., Harris, I.S., and Mak, T.W. (2011). Regulation of cancer cell metabolism. Nat Rev Cancer *11*, 85-95.

Camp Jr, C.H., and Cicerone, M.T. (2015). Chemically sensitive bioimaging with coherent Raman scattering. Nature Photonics *9*, 295-305.

Cassada, R.C., and Russell, R.L. (1975). The dauerlarva, a post-embryonic developmental variant of the nematode Caenorhabditis elegans. Dev Biol *46*, 326-342.

Chen, A.T., Guo, C., Itani, O.A., Budaitis, B.G., Williams, T.W., Hopkins, C.E., McEachin, R.C., Pande, M., Grant, A.R., Yoshina, S.*, et al.* (2015). Longevity Genes Revealed by Integrative Analysis of Isoform-Specific daf-16/FoxO Mutants of Caenorhabditis elegans. Genetics *201*, 613-629.

Cunningham, K.A., Bouagnon, A.D., Barros, A.G., Lin, L., Malard, L., Romano-Silva, M.A., and Ashrafi, K. (2014). Loss of a neural AMP-activated kinase mimics the effects of elevated serotonin on fat, movement, and hormonal secretions. PLoS Genet *10*, e1004394.

bioRxiv preprint doi: https://doi.org/10.1101/323956; this version posted May 16, 2018. The copyright holder for this preprint (which was not certified by peer review) is the author/funder. All rights reserved. No reuse allowed without permission.

Depuydt, G., Xie, F., Petyuk, V.A., Smolders, A., Brewer, H.M., Camp, D.G., 2nd, Smith, R.D., and Braeckman, B.P. (2014). LC-MS proteomics analysis of the insulin/IGF-1-deficient Caenorhabditis elegans daf-2(e1370) mutant reveals extensive restructuring of intermediary metabolism. J Proteome Res *13*, 1938-1956.

Erkut, C., Gade, V.R., Laxman, S., and Kurzchalia, T.V. (2016). The glyoxylate shunt is essential for desiccation tolerance in C. elegans and budding yeast. eLife *5*.

Erkut, C., and Kurzchalia, T.V. (2015). The C. elegans dauer larva as a paradigm to study metabolic suppression and desiccation tolerance. Planta.

Fielenbach, N., and Antebi, A. (2008). C. elegans dauer formation and the molecular basis of plasticity. Genes Dev *22*, 2149-2165.

Fisher, A.L., and Lithgow, G.J. (2006). The nuclear hormone receptor DAF-12 has opposing effects on Caenorhabditis elegans lifespan and regulates genes repressed in multiple long-lived worms. Aging Cell *5*, 127-138.

Fuchs, S., Bundy, J.G., Davies, S.K., Viney, J.M., Swire, J.S., and Leroi, A.M. (2010). A metabolic signature of long life in Caenorhabditis elegans. BMC Biol *8*, 14.

Gems, D., Sutton, A.J., Sundermeyer, M.L., Albert, P.S., King, K.V., Edgley, M.L., Larsen, P.L., and Riddle, D.L. (1998). Two pleiotropic classes of daf-2 mutation affect larval arrest, adult behavior, reproduction and longevity in Caenorhabditis elegans. Genetics *150*, 129-155.

Hand, S.C., Denlinger, D.L., Podrabsky, J.E., and Roy, R. (2016). Mechanisms of animal diapause: recent developments from nematodes, crustaceans, insects, and fish. American journal of physiology Regulatory, integrative and comparative physiology *310*, R1193-1211.

Hannich, J.T., Entchev, E.V., Mende, F., Boytchev, H., Martin, R., Zagoriy, V., Theumer, G., Riezman, I., Riezman, H., Knolker, H.J., *et al*. (2009). Methylation of

bioRxiv preprint doi: https://doi.org/10.1101/323956; this version posted May 16, 2018. The copyright holder for this preprint (which was not certified by peer review) is the author/funder. All rights reserved. No reuse allowed without permission.

the sterol nucleus by STRM-1 regulates dauer larva formation in Caenorhabditis elegans. Dev Cell *16*, 833-843.

Henderson, S.T., and Johnson, T.E. (2001). daf-16 integrates developmental and environmental inputs to mediate aging in the nematode Caenorhabditis elegans. Curr Biol *11*, 1975-1980.

Hermann, G.J., Schroeder, L.K., Hieb, C.A., Kershner, A.M., Rabbitts, B.M., Fonarev, P., Grant, B.D., and Priess, J.R. (2005). Genetic analysis of lysosomal trafficking in Caenorhabditis elegans. Mol Biol Cell *16*, 3273-3288.

Hibshman, J.D., Doan, A.E., Moore, B.T., Kaplan, R.E., Hung, A., Webster, A.K., Bhatt, D.P., Chitrakar, R., Hirschey, M.D., and Baugh, L.R. (2017). daf-16/FoxO promotes gluconeogenesis and trehalose synthesis during starvation to support survival. eLife *6*.

Holt, S.J., and Riddle, D.L. (2003). SAGE surveys C. elegans carbohydrate metabolism: evidence for an anaerobic shift in the long-lived dauer larva. Mech Ageing Dev *124*, 779-800.

Homem, C.C., Steinmann, V., Burkard, T.R., Jais, A., Esterbauer, H., and Knoblich, J.A. (2014). Ecdysone and mediator change energy metabolism to terminate proliferation in Drosophila neural stem cells. Cell *158*, 874-888.

Houthoofd, K., Braeckman, B.P., Lenaerts, I., Brys, K., De Vreese, A., Van Eygen, S., and Vanfleteren, J.R. (2002). Ageing is reversed, and metabolism is reset to young levels in recovering dauer larvae of C. elegans. Exp Gerontol *37*, 1015-1021.

Ito, K., and Suda, T. (2014). Metabolic requirements for the maintenance of self-renewing stem cells. Nature reviews Molecular cell biology *15*, 243-256.

Jungst, C., Winterhalder, M.J., and Zumbusch, A. (2011). Fast and long term lipid droplet tracking with CARS microscopy. J Biophotonics *4*, 435-441.

bioRxiv preprint doi: https://doi.org/10.1101/323956; this version posted May 16, 2018. The copyright holder for this preprint (which was not certified by peer review) is the author/funder. All rights reserved. No reuse allowed without permission.

Kaplan, R.E., Chen, Y., Moore, B.T., Jordan, J.M., Maxwell, C.S., Schindler, A.J., and Baugh, L.R. (2015). dbl-1/TGF-beta and daf-12/NHR Signaling Mediate Cell-Nonautonomous Effects of daf-16/FOXO on Starvation-Induced Developmental Arrest. PLoS Genet *11*, e1005731.

Kemp, R., and Guan, Y. (1997). Heat flux and the calorimetric-respirometric ratio as measures of catabolic flux in mammalian cells. Thermochimica Acta *300*, 199-211.

Lee, R.Y., Hench, J., and Ruvkun, G. (2001). Regulation of C. elegans DAF-16 and its human ortholog FKHRL1 by the daf-2 insulin-like signaling pathway. Curr Biol *11*, 1950-1957.

Lin, K., Hsin, H., Libina, N., and Kenyon, C. (2001). Regulation of the Caenorhabditis elegans longevity protein DAF-16 by insulin/IGF-1 and germline signaling. Nat Genet *28*, 139-145.

Luz, A.T., Godebo, T.R., Bhatt, D.P., Ilkayeva, O.R., Maurer, L.L., Hirschey, M.D., and Meyer, J.N. (2016). Arsenite Uncouples Mitochondrial Respiration and Induces a Warburg-Like Effect in Caenorhabditis elegans. Toxicol Sci *154*, 195.

Madi, A., Mikkat, S., Koy, C., Ringel, B., Thiesen, H.J., and Glocker, M.O. (2008). Mass spectrometric proteome analysis suggests anaerobic shift in metabolism of Dauer larvae of Caenorhabditis elegans. Biochimica et biophysica acta *1784*, 1763-1770.

Martins, R., Lithgow, G.J., and Link, W. (2016). Long live FOXO: unraveling the role of FOXO proteins in aging and longevity. Aging Cell *15*, 196-207.

Matyash, V., Entchev, E.V., Mende, F., Wilsch-Brauninger, M., Thiele, C., Schmidt, A.W., Knolker, H.J., Ward, S., and Kurzchalia, T.V. (2004). Sterol-derived hormone(s) controls entry into diapause in Caenorhabditis elegans by consecutive activation of DAF-12 and DAF-16. PLoS biology *2*, e280.

bioRxiv preprint doi: https://doi.org/10.1101/323956; this version posted May 16, 2018. The copyright holder for this preprint (which was not certified by peer review) is the author/funder. All rights reserved. No reuse allowed without permission.

Moreno-Arriola, E., El Hafidi, M., Ortega-Cuellar, D., and Carvajal, K. (2016). AMP-Activated Protein Kinase Regulates Oxidative Metabolism in Caenorhabditis elegans through the NHR-49 and MDT-15 Transcriptional Regulators. PLoS One *11*, e0148089.

Moroz, N., Carmona, J.J., Anderson, E., Hart, A.C., Sinclair, D.A., and Blackwell, T.K. (2014). Dietary restriction involves NAD(+) -dependent mechanisms and a shift toward oxidative metabolism. Aging Cell *13*, 1075-1085.

Motola, D.L., Cummins, C.L., Rottiers, V., Sharma, K.K., Li, T., Li, Y., Suino-Powell, K., Xu, H.E., Auchus, R.J., Antebi, A., *et al*. (2006). Identification of ligands for DAF-12 that govern dauer formation and reproduction in C. elegans. Cell *124*, 1209-1223.

Murphy, C.T., McCarroll, S.A., Bargmann, C.I., Fraser, A., Kamath, R.S., Ahringer, J., Li, H., and Kenyon, C. (2003). Genes that act downstream of DAF-16 to influence the lifespan of Caenorhabditis elegans. Nature *424*, 277-283.

Narbonne, P., and Roy, R. (2006). Inhibition of germline proliferation during C. elegans dauer development requires PTEN, LKB1 and AMPK signalling. Development *133*, 611-619.

Narbonne, P., and Roy, R. (2009). Caenorhabditis elegans dauers need LKB1/AMPK to ration lipid reserves and ensure long-term survival. Nature *457*, 210-214.

Penkov, S., Kaptan, D., Erkut, C., Sarov, M., Mende, F., and Kurzchalia, T.V. (2015). Integration of carbohydrate metabolism and redox state controls dauer larva formation in Caenorhabditis elegans. Nature communications *6*, 8060.

Penkov, S., Mende, F., Zagoriy, V., Erkut, C., Martin, R., Passler, U., Schuhmann, K., Schwudke, D., Gruner, M., Mantler, J., *et al*. (2010). Maradolipids: diacyltrehalose

bioRxiv preprint doi: https://doi.org/10.1101/323956; this version posted May 16, 2018. The copyright holder for this preprint (which was not certified by peer review) is the author/funder. All rights reserved. No reuse allowed without permission.

glycolipids specific to dauer larva in Caenorhabditis elegans. Angew Chem Int Ed Engl *49*, 9430-9435.

Possik, E., Ajisebutu, A., Manteghi, S., Gingras, M.C., Vijayaraghavan, T., Flamand, M., Coull, B., Schmeisser, K., Duchaine, T., van Steensel, M., *et al*. (2015). FLCN and AMPK Confer Resistance to Hyperosmotic Stress via Remodeling of Glycogen Stores. PLoS Genet *11*, e1005520.

Riddle, D.L. (1988). 12 The Dauer Larva. Cold Spring Harbor Monograph Archive *17*, 393-412.

Riddle, D.L., and Albert, P.S. (1997). Genetic and environmental regulation of dauer larva development. In *Celegans* II, D.L. Riddle, T. Blumenthal, J.B. Meyer, and J.R. Priess, eds. (Cold Spring Harbor Laboratory Press), pp. 739-768.

Riddle, D.L., Swanson, M.M., and Albert, P.S. (1981). Interacting genes in nematode dauer larva formation. Nature *290*, 668-671.

Seo, Y., Kingsley, S., Walker, G., Mondoux, M.A., and Tissenbaum, H.A. (2018). Metabolic shift from glycogen to trehalose promotes lifespan and healthspan in Caenorhabditis elegans. Proc Natl Acad Sci U S A *115*, E2791-E2800.

Sheaffer, K.L., Updike, D.L., and Mango, S.E. (2008). The Target of Rapamycin pathway antagonizes pha-4/FoxA to control development and aging. Curr Biol *18*, 1355-1364.

Smith, D.G., and Sturmey, R.G. (2013). Parallels between embryo and cancer cell metabolism (Portland Press Limited).

Tullet, J.M., Araiz, C., Sanders, M.J., Au, C., Benedetto, A., Papatheodorou, I., Clark, E., Schmeisser, K., Jones, D., Schuster, E.F., *et al*. (2014). DAF-16/FoxO directly regulates an atypical AMP-activated protein kinase gamma isoform to mediate the

bioRxiv preprint doi: https://doi.org/10.1101/323956; this version posted May 16, 2018. The copyright holder for this preprint (which was not certified by peer review) is the author/funder. All rights reserved. No reuse allowed without permission.

effects of insulin/IGF-1 signaling on aging in Caenorhabditis elegans. PLoS Genet *10*, e1004109.

Vanfleteren, J.R., and De Vreese, A. (1996). Rate of aerobic metabolism and superoxide production rate potential in the nematode Caenorhabditis elegans. J Exp Zool *274*, 93-100.

Vowels, J.J., and Thomas, J.H. (1992). Genetic analysis of chemosensory control of dauer formation in Caenorhabditis elegans. Genetics *130*, 105-123.

Wadsworth, W.G., and Riddle, D.L. (1989). Developmental regulation of energy metabolism in Caenorhabditis elegans. Dev Biol *132*, 167-173.

Wang, J., and Kim, S.K. (2003). Global analysis of dauer gene expression in Caenorhabditis elegans. Development *130*, 1621-1634.

Warburg, O. (1956). On the origin of cancer cells. Science *123*, 309-314.

Weir, H.J., Yao, P., Huynh, F.K., Escoubas, C.C., Goncalves, R.L., Burkewitz, K., Laboy, R., Hirschey, M.D., and Mair, W.B. (2017). Dietary Restriction and AMPK Increase Lifespan via Mitochondrial Network and Peroxisome Remodeling. Cell metabolism *26*, 884-896 e885.

Williams, R.M., Zipfel, W.R., and Webb, W.W. (2005). Interpreting second-harmonic generation images of collagen I fibrils. Biophys J *88*, 1377-1386.

Wullschleger, S., Loewith, R., and Hall, M.N. (2006). TOR signaling in growth and metabolism. Cell *124*, 471-484.

Xie, M., and Roy, R. (2012). Increased levels of hydrogen peroxide induce a HIF-1-dependent modification of lipid metabolism in AMPK compromised C. elegans dauer larvae. Cell metabolism *16*, 322-335.

bioRxiv preprint doi: https://doi.org/10.1101/323956; this version posted May 16, 2018. The copyright holder for this preprint (which was not certified by peer review) is the author/funder. All rights reserved. No reuse allowed without permission.

Xie, M., and Roy, R. (2015a). AMP-Activated Kinase Regulates Lipid Droplet Localization and Stability of Adipose Triglyceride Lipase in C. elegans Dauer Larvae. PLoS One *10*, e0130480.

Xie, M., and Roy, R. (2015b). The Causative Gene in Chanarian Dorfman Syndrome Regulates Lipid Droplet Homeostasis in C. elegans. PLoS Genet *11*, e1005284.

Zarse, K., Schmeisser, S., Groth, M., Priebe, S., Beuster, G., Kuhlow, D., Guthke, R., Platzer, M., Kahn, C.R., and Ristow, M. (2012). Impaired insulin/IGF1 signaling extends life span by promoting mitochondrial L-proline catabolism to induce a transient ROS signal. Cell metabolism *15*, 451-465.

bioRxiv preprint doi: https://doi.org/10.1101/323956; this version posted May 16, 2018. The copyright holder for this preprint (which was not certified by peer review) is the author/funder. All rights reserved. No reuse allowed without permission.

Figure legends

Figure 1. DAF-16 mediates the switch to low metabolic rate in dauer formation.

(A) Signaling pathways that trigger dauer formation. In the absence of insulin-like peptides, DAF-2 is suppressed, leading to activation of DAF-16. In parallel, dauer-inducing pheromones inhibit the TGF-β and guanylyl cyclase pathways, and this lowers the production of DAs by DAF-9, resulting in activated DAF-12. DAF-16 stimulates DAF-12 by inhibiting DAF-9 but DAF-12 is also capable of activating DAF-16. DAF-16 and DAF-12 control different subsets of genes designated X′Y′Z′ and X′′Y′′Z′′, respectively.

(B) Formation of L3 arrested larvae of *daf-2;daf-12* or DA-fed *daf-2* at restrictive temperature. The reduction of DAF-2 activity leads to activation of DAF-16. DAF-16 also inhibits DAF-9 activity but this effect is neutralized by the *daf-12* mutation or the addition of exogenous DA. Thus, DAF-16 is active but DAF-12 is not.

(C) Formation of dauer-like larvae of *daf-16* on 4-MS. DAF-12 is activated due to a lack of substrates for DA synthesis; however, DAF-16 activity is absent due to the mutation in the *daf-16* locus.

(**D**) Continuous measurement of the heat dissipated in unit time (heat flow) by wild-type (N2) worms undergoing reproductive growth on cholesterol or dauer formation on 4-MS. After 24 hours, worms entering dauer state switch to lower heat production.

(**E**) Heat flow of *daf-2, daf-2;daf-12* and *daf-2;daf-16* grown at 25˚C. *daf-16,* but not *daf-12*, suppresses the switch to lower heat production observed in *daf-2*.

Panels **D** and **E** show representative diagrams from 4 experiments with 1-4 technical replicates. chol – cholesterol, 4-MS – 4-methylated sterol, DA – dafachronic acid.

bioRxiv preprint doi: https://doi.org/10.1101/323956; this version posted May 16, 2018. The copyright holder for this preprint (which was not certified by peer review) is the author/funder. All rights reserved. No reuse allowed without permission.

Figure 2. Arrested *daf-2;daf-12* larvae have L3 larval morphology.

(**A**) Transmission electron micrograph of a cross-section of a growing L3 larva of *daf-2* grown at 15˚C. The left panel represents an overview of the body organization. Note the low number of lipid droplets (arrowhead). The gut lumen is elongated and lined by multiple, densely packed microvilli (high magnification image in the central panel, corresponding to the large rectangle in the left panel). The structure of the cuticle is displayed on the right panel, corresponding to the small rectangle in the left panel. Note the absence of a striated circular layer.

(**B**) Electron micrograph of a *daf-2* dauer larva grown at 25˚C. The left panel shows that the body is radially constricted, shows extensive accumulation of lipid droplets (arrowheads) and dauer-specific alae (arrows). The gut lumen is rounded, microvilli are almost absent (central panel, large rectangle in left panel). The cuticle possesses a striated layer (right panel and indicated by a bracket, small rectangle in the left panel).

(**C**) Electron micrograph of a *daf-2;daf-12* arrested larva grown at 25˚C. The body is not radially constricted but displays extensive accumulation of lipid droplets (left panel, arrowheads). Alae are absent (left panel). The gut lumen (central panel, large rectangle in left panel) and the cuticle (right panel, small rectangle in left panel) structurally resemble the ones displayed by L3 growing larvae as shown in (**A**).

Scale bars in **A**, **B** and **C** correspond to 5 μm (left panels), 1 μm (central panels) and 0.5 μm (right panels). Representative images of at least five animals per condition.

bioRxiv preprint doi: https://doi.org/10.1101/323956; this version posted May 16, 2018. The copyright holder for this preprint (which was not certified by peer review) is the author/funder. All rights reserved. No reuse allowed without permission.

Figure 3. DAF-16 determines the energy expenditure and lifespan of dauer larvae

(**A**) Continuous measurement of the cumulative heat dissipation by *daf-2* dauers and *daf-2;daf-12* arrested L3 larvae grown at 25˚C in the period after the developmental arrest is completed. The two strains produce comparable amounts of heat.

(**B**) Cumulative heat dissipation by wild-type (N2) dauers and *daf-16* dauer-like larvae grown on 4-MS in the period after the developmental arrest is completed. *daf-16* produces substantially more heat than N2.

(**C**) CARS microscopy of lipid droplets (red) in *daf-2* dauers and *daf-2;daf-12* arrested L3 larvae grown at 25˚C, and wild-type (N2) dauers and *daf-16* dauer-like larvae grown on 4-MS in the period after the developmental arrest is completed. While the *daf-2*, *daf-2;daf-12* and wild-type animals show good lipid droplet conservation, in *daf-16* the lipid droplets are almost undetectable after 2 days of arrest. Note that the lysosome-related organelles (green autofluorescence) are not a source of CARS signal under the conditions used.

(**D**) Survival rate of *daf-2* dauers and *daf-2;daf-12* arrested L3 larvae grown at 25˚C, and wild-type (N2) dauers and *daf-16* dauer-like larvae grown on 4-MS in buffer. The *daf-16* animals show very early mortality.

4-MS – 4-methylated sterol, CARS – Coherent Anti-Stokes Raman Scattering, SHG – Second Harmonic Generation. In (**A**) and (**B**), representative diagrams of at least 2 experiments with 3 replicates. In (**C**), representative images of at least 6 animals, scale bars – 10 μm. In (**D**), data is represented as means ± 95% confidence intervals of 3 experiments with 3 replicates. *** significance of $p<0.001$; ns - no significant difference determined by log-rank test.

bioRxiv preprint doi: https://doi.org/10.1101/323956; this version posted May 16, 2018. The copyright holder for this preprint (which was not certified by peer review) is the author/funder. All rights reserved. No reuse allowed without permission.

Figure 4. AAK-2 regulates the energy expenditure in dauer state.

(A) Electron microscopy of *daf-2;aak-2(gt33)* animals. Both animals collected on the day of dauer formation and after five days of incubation at 25 ˚C display typical dauer features such as alae (upper panels, arrows) and striated layers of the cuticle (lower panels). On the upper panels is visible that five day-old dauers show features of starvation: shrinkage of the volume of the hypodermis (H), expansion of the pseudocoelomic cavity (one asterisk), formation of a cavity between the cuticle and the hypodermis (two asterisks) and widening of the gut lumen (three asterisks). In addition, the animals show much fewer mitochondria which are substantially enlarged (arrowheads).

(B) TLC of ^{14}C-acetate labelled TGs, PEs (major representatives of the membrane phospholipids) and trehalose from *daf-2* and *daf-2;aak-2* dauers measured at different time points after the arrest. Both strains preserve PEs to a similar extent. However, unlike *daf-2*, dauers of *daf-2;aak-2* are depleted of TGs and trehalose very rapidly.

(**C**) Quantification of the band intensities in (**A**) represented by peak area of the optical density.

TG – triglycerides, PE – phosphatidylethanolamine, Tre – trehalose, RU – relative units, DA – dafachronic acid. In (**A**), Scale bars 5 μm (upper panels) and 0.5 μm (lower bars); representative images of at least 4 animals. In (**C**) data is represented as means ± SD of 2 experiments with 3 replicates. *** $p<0.001$; ** $p<0.01$; * $p<0.1$; ns - no significant difference determined by Student t-test.

bioRxiv preprint doi: https://doi.org/10.1101/323956; this version posted May 16, 2018. The copyright holder for this preprint (which was not certified by peer review) is the author/funder. All rights reserved. No reuse allowed without permission.

Figure 5. Animals with active DAF-16 maintain nucleolar localization of FIB-1 in an AAK-2 dependent manner.

(**A**) Maximum intensity Z-projection of the eGFP fluorescence in *daf-2;fib-1::GFP* dauers at different time points after dauer arrest. FIB-1 is localized to the nuclei (asterisks) with highest concentration in the nucleoli in all cells. Over time, this localization is retained.

(**B**) Detection of FIB-1::eGFP in *daf-2;fib-1::GFP* arrested L3 larvae grown on DA at different time points after the arrest. Over time, the animals maintain nucleolar localization of FIB-1.

(C) Detection of FIB-1::eGFP in *daf-2;aak-2;fib-1::GFP* dauers at different time points after arrest. Early after arrest, FIB-1 is localized to the nucleoli. After 4 days, FIB-1 is still detected in the nucleoli but also in multiple smaller granules dispersed in the nucleoplasm of some cells (arrow). After 7 days, FIB-1 is almost completely dissolved in the nucleoplasm of most of the cells (arrowheads).

In all panels scale bars – 5 μm. Representative images of 3 experiments with at least 7 animals.

Figure 6. DAF-16 and DAF-12 independently induce a gluconeogenic mode.

(**A**) 2D-TLC of ^{14}C-acetate-labelled metabolites from *daf-2* dauers and *daf-2;daf-12* arrested larvae grown at 25˚C compared to growing L3 larvae of the same strains grown at 15˚C. Note the accumulation of trehalose (1) in the arrested stages, indicating a switch from TCA cycle to gluconeogenesis.

(**B**) 2D-TLC of ^{14}C-acetate-labelled metabolites from wild-type (N2) dauers and *daf-16* dauer-like larvae grown on 4-MS compared to growing L3 larvae of the same

bioRxiv preprint doi: https://doi.org/10.1101/323956; this version posted May 16, 2018. The copyright holder for this preprint (which was not certified by peer review) is the author/funder. All rights reserved. No reuse allowed without permission.

strains grown on cholesterol. Again, both types of dauer(-like) larvae display intensive gluconeogenesis as indicated by the accumulation of trehalose (1).
Chol – cholesterol, 4-MS – 4-methylated sterol, 1 – trehalose, 2 – glucose, 3 – glutamate, 4 – glycine/serine, 5 – glutamate, 6 – alanine/threonine. Representative images from at least 2 experiments.

Figure 7. AAK-2 induces a gluconeogenic mode and growth arrest downstream of DAF-16.

(**A**) 2D-TLC of ^{14}C-acetate-labelled metabolites from *daf-2;aak-2* L3 larvae grown at 15˚C, dauers grown at 25˚C and L3 larvae obtained at 25˚C in the presence of DA. Dauers of this strain are in gluconeogenic mode. L3 larvae grown at 25˚C on DA, however, do not accumulate trehalose (1), indicating an active TCA cycle.
(**B**) Micrographs of *daf-2* and *daf-2;aak-2* animals grown at 25˚C in the presence or absence of DA. Inhibition of DAF-12 promotes reproductive growth in *daf-2;aak-2* but not in *daf-2*.
(**C**) Quantification of the larval arrest in (**B**).
DA – dafachronic acid, 1 – trehalose, 2 – glucose, 3 – glutamate, 4 – glycine/serine, 5 – glutamate, 6 – alanine/threonine. Representative images from at least 2 experiments. In (**C**) data is represented as means ± 95% confidence intervals of 3 experiments with 3 replicates. *** $p<0.001$; ns - no significant difference determined by one-way analysis of variance.

bioRxiv preprint doi: https://doi.org/10.1101/323956; this version posted May 16, 2018. The copyright holder for this preprint (which was not certified by peer review) is the author/funder. All rights reserved. No reuse allowed without permission.

Figure 8. Model of the regulation of metabolism and growth in reproductive and dauer development.

In both panels, environmental and internal stimuli regulate the secretion of insulin-like peptides that activate DAF-2, leading to inhibition of DAF-16 and, downstream or in parallel to it, AAK-2. The TGF-β and guanylyl cyclase pathways stimulate the production of DAs by DAF-9 which inhibits DAF-12. DAF-16 inhibits global catabolism via or in parallel to AAK-2, limiting the depletion of internal energy reserves and the production of building blocks and energy for anabolic processes. The expression of dauer-specific genes is under DAF-12 control. DAF-16 and AAK-2 inhibit the TCA cycle and induce gluconeogenesis. DAF-12 is also capable of inducing gluconeogenic mode independently of DAF-16 or AAK-2. The TCA cycle provides energy through oxidative phosphorylation (OXPHOS) and building blocks for anabolic reactions.

(**A**) When conditions favor reproductive growth, DAF-16, AAK-2 and DAF-12 are inhibited, and the catabolism of nutrients and the TCA cycle are stimulated, whereas gluconeogenesis and the expression of dauer-specific genes are kept low. The TCA cycle and the enhanced catabolism provide energy and intermediates for biosynthetic reactions. The overall levels of anabolism are high, which allows for continuous growth.

(**B**) In dauer formation, DAF-16, AAK-2 and DAF-12 are active, which inhibits the TCA cycle and promotes gluconeogenesis. DAF-16 and AAK-2 limit the catabolism of internal energy reserves, while the expression of dauer-specific genes promoted by DAF-12 drives dauer morphogenesis. The levels of anabolism are low due to the inhibited TCA cycle and generally low catabolism. Growth is suppressed, the worms keep energy expenditure at low levels and enter a long-lasting dauer state.

bioRxiv preprint doi: https://doi.org/10.1101/323956; this version posted May 16, 2018. The copyright holder for this preprint (which was not certified by peer review) is the author/funder. All rights reserved. No reuse allowed without permission.

Figure 1.

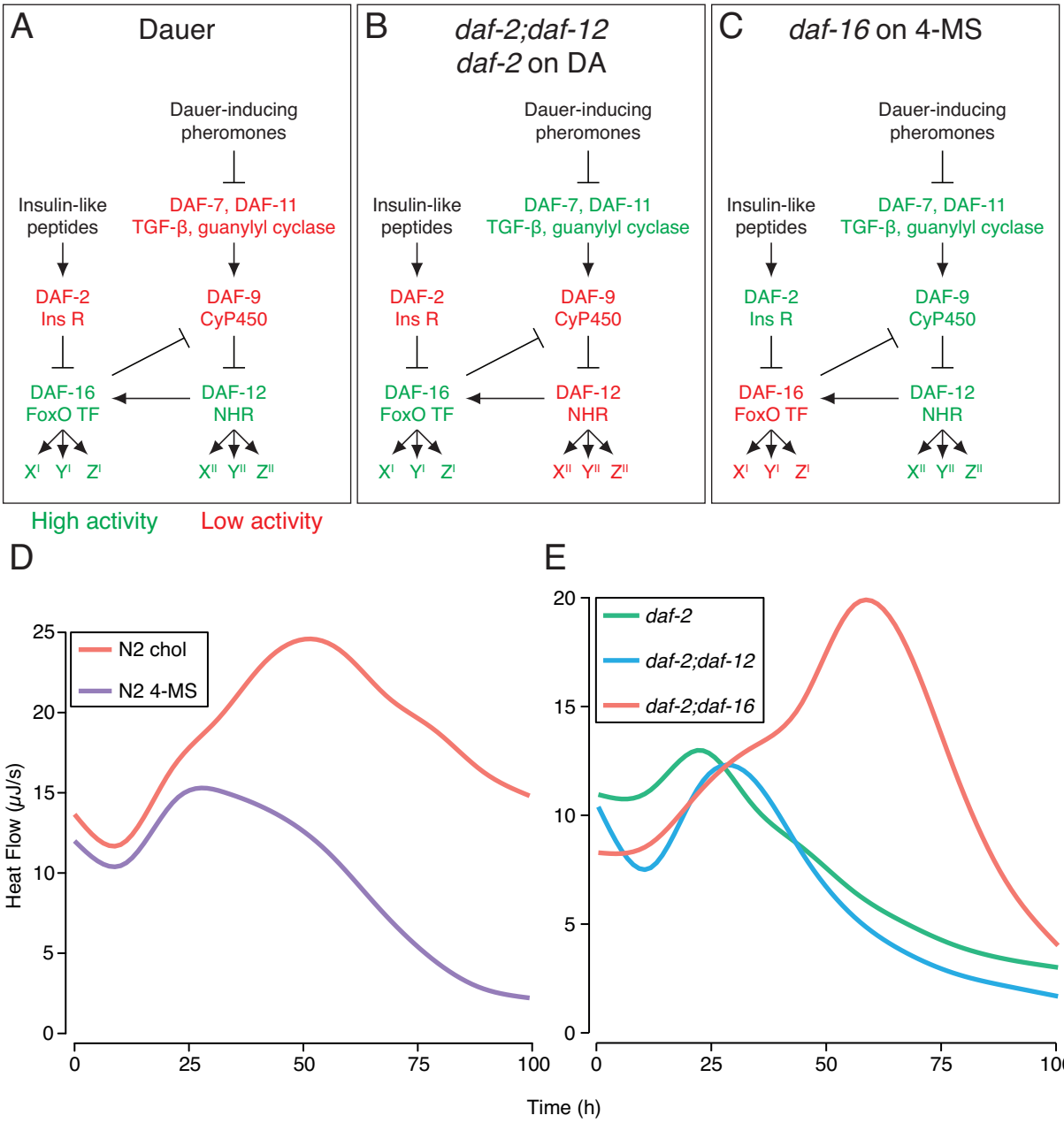

bioRxiv preprint doi: https://doi.org/10.1101/323956; this version posted May 16, 2018. The copyright holder for this preprint (which was not certified by peer review) is the author/funder. All rights reserved. No reuse allowed without permission.

Figure 2.

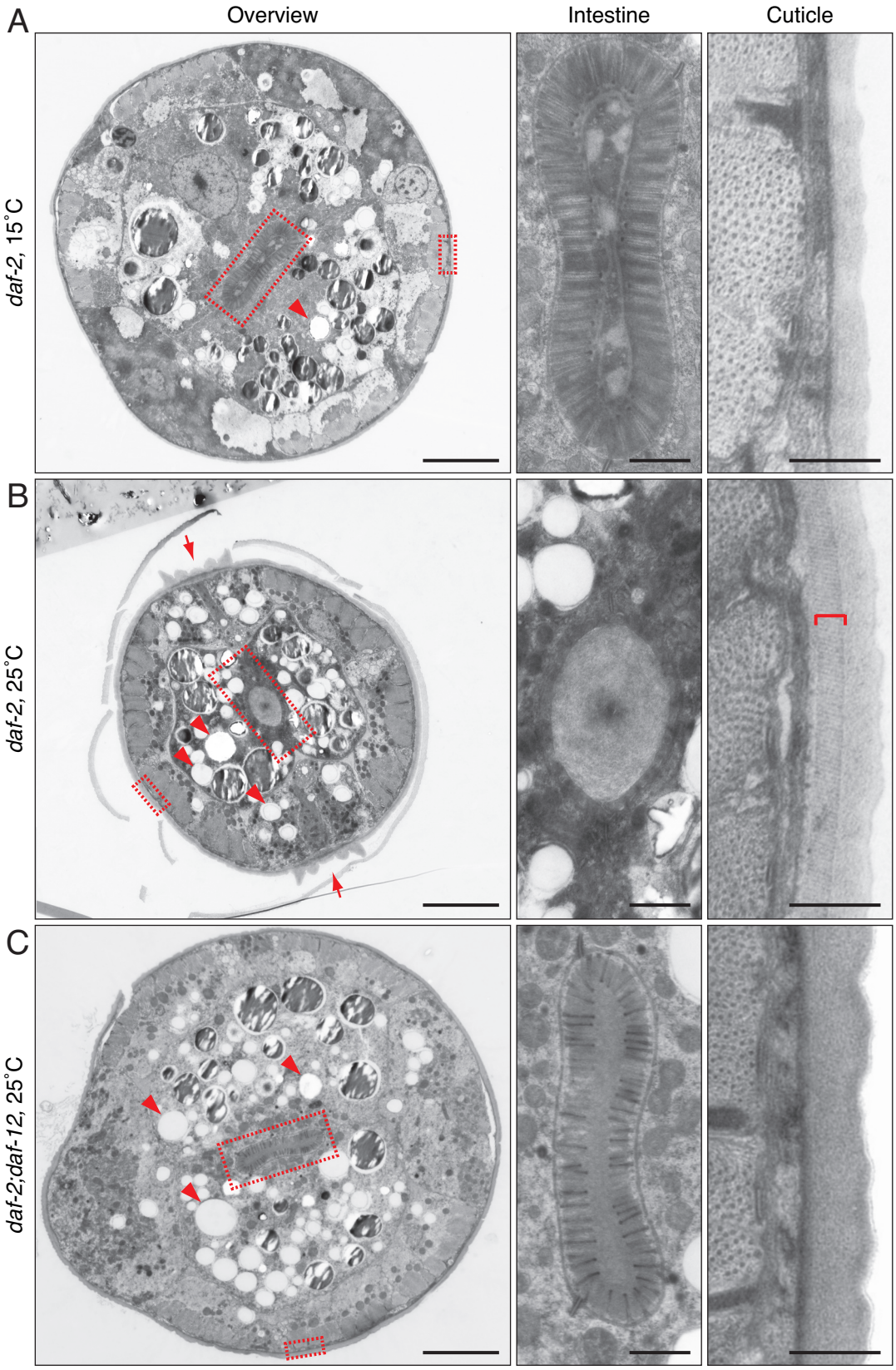

bioRxiv preprint doi: https://doi.org/10.1101/323956; this version posted May 16, 2018. The copyright holder for this preprint (which was not certified by peer review) is the author/funder. All rights reserved. No reuse allowed without permission.

Figure 3.

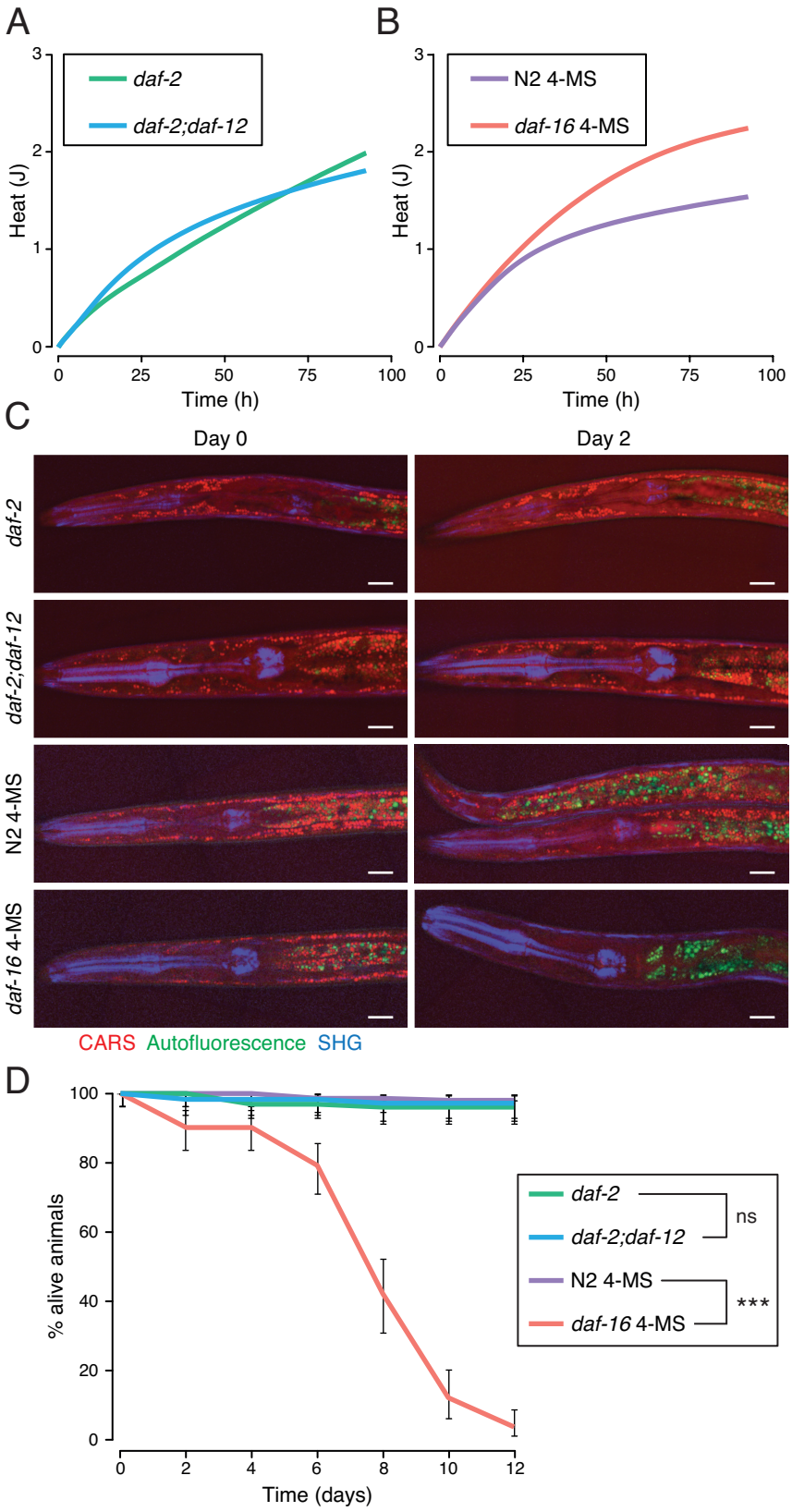

bioRxiv preprint doi: https://doi.org/10.1101/323956; this version posted May 16, 2018. The copyright holder for this preprint (which was not certified by peer review) is the author/funder. All rights reserved. No reuse allowed without permission.

Figure 4.

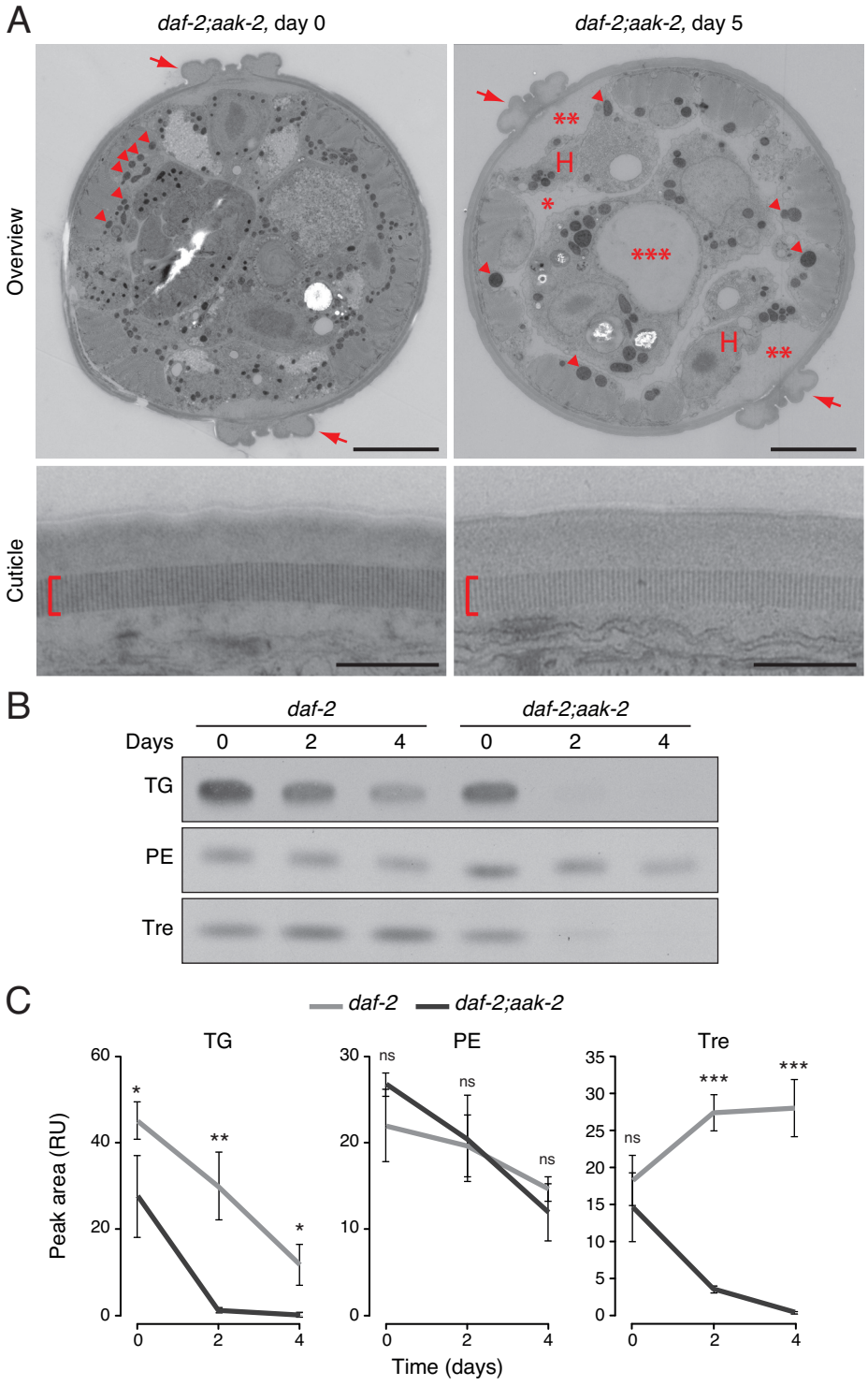

bioRxiv preprint doi: https://doi.org/10.1101/323956; this version posted May 16, 2018. The copyright holder for this preprint (which was not certified by peer review) is the author/funder. All rights reserved. No reuse allowed without permission.

Figure 5.

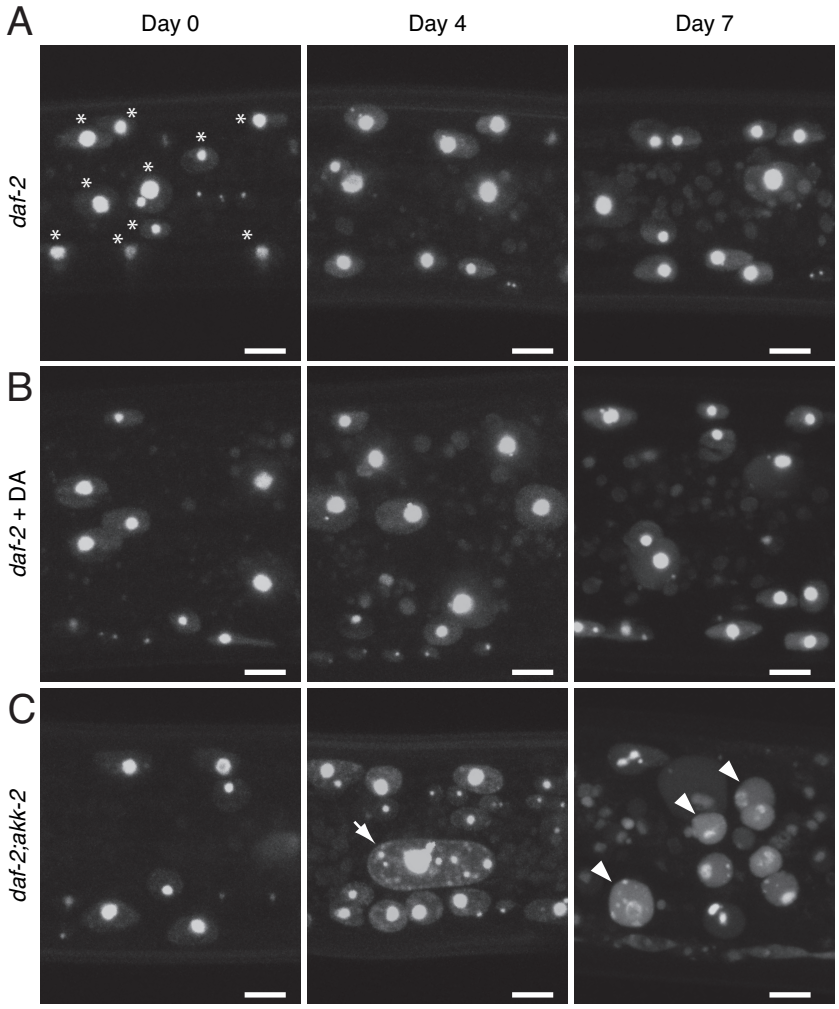

bioRxiv preprint doi: https://doi.org/10.1101/323956; this version posted May 16, 2018. The copyright holder for this preprint (which was not certified by peer review) is the author/funder. All rights reserved. No reuse allowed without permission.

Figure 6.

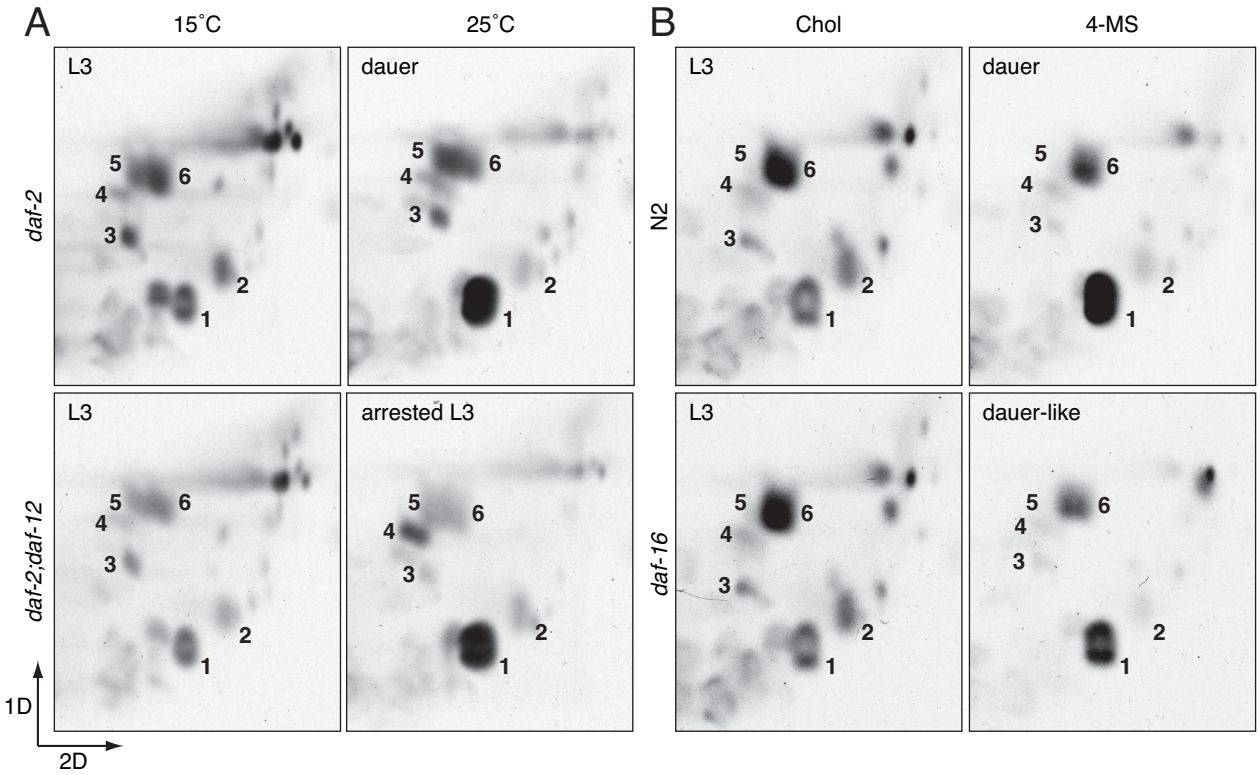

bioRxiv preprint doi: https://doi.org/10.1101/323956; this version posted May 16, 2018. The copyright holder for this preprint (which was not certified by peer review) is the author/funder. All rights reserved. No reuse allowed without permission.

Figure 7.

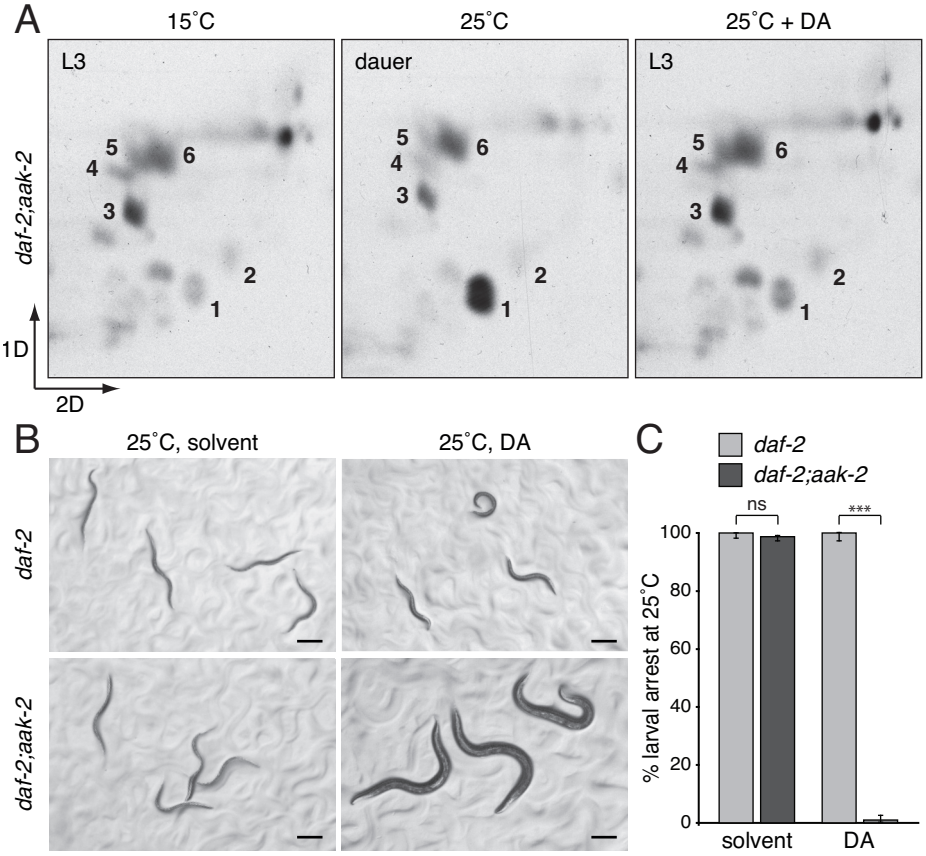

bioRxiv preprint doi: https://doi.org/10.1101/323956; this version posted May 16, 2018. The copyright holder for this preprint (which was not certified by peer review) is the author/funder. All rights reserved. No reuse allowed without permission.

Figure 8.